Candida auris undergoes adhesin-dependent and -independent cellular aggregation

Chloe Pelletier[1,2,4], **Sophie Shaw**[3,5], **Sakinah Alsayegh**[1], **Alistair J. P. Brown**[2], and **Alexander Lorenz**[1,*]

[1]Institute of Medical Sciences (IMS), University of Aberdeen, Aberdeen, UK

[2]MRC Centre for Medical Mycology, University of Exeter, Exeter, UK

[3]Centre for Genome-Enabled Biology and Medicine (CGEBM), University of Aberdeen, Aberdeen, UK

[4]Present Address: Wellcome Centre for Anti-Infectives Research, School of Life Sciences, University of Dundee, Dundee, UK

[5]Present Address: All Wales Medical Genomics Service, Institute of Medical Genetics, University Hospital of Wales, Cardiff, UK

*Correspondence should be addressed to

Alexander Lorenz

Institute of Medical Sciences (IMS)

University of Aberdeen

Foresterhill

Aberdeen AB25 2ZD

United Kingdom

E-mail: a.lorenz@abdn.ac.uk

ORCIDs: 0000-0002-5581-3442 (CP), 0000-0003-2367-2670 (SS), 0000-0003-1406-4251 (AJPB), 0000-0003-1925-3713 (AL)

28

Abstract

Candida auris is a fungal pathogen of humans responsible for nosocomial infections with high mortality rates. High levels of resistance to antifungal drugs and environmental persistence mean these infections are difficult to treat and eradicate from a healthcare setting. Understanding the life cycle and the genetics of this fungus underpinning clinically relevant traits, such as antifungal resistance and virulence, is of the utmost importance to develop novel treatments and therapies. Epidemiological and genomic studies have identified five geographical clades (I-V), which display phenotypic and genomic differences. Aggregation of cells, a phenotype primarily of clade III strains, has been linked to reduced virulence in mouse and *Galleria mellonella* infection models. The aggregation phenotype has thus been associated with conferring an advantage for (skin) colonisation rather than for systemic infection. However, strains with different clade affiliations were compared to infer the effects of different morphologies on virulence. This makes it difficult to distinguish morphology-dependent causes from clade-specific or even strain-specific genetic factors. Here, we identify two different types of aggregation: one induced by antifungal treatment which is a result of a cell separation defect; and a second which is controlled by growth conditions and only occurs in strains with the ability to aggregate. The latter aggregation type depends on an ALS-family adhesin which is differentially expressed during aggregation in an aggregative *C. auris* strain. Finally, we demonstrate that macrophages cannot clear aggregates, suggesting that aggregation might after all provide a benefit during systemic infection and could facilitate long-term persistence in the host.

Key words: *Candida auris*, adhesin, cell aggregation, virulence.

Author Summary

Candida auris is a single-celled fungus, a yeast, that can cause severe infections in hospital patients. This fungus is difficult to treat because it is resistant to many antifungal drugs. Therefore, to understand the processes that enhance the virulence of this yeast with a view to developing new treatments. Previous studies have found that *C. auris* can form aggregates, or clumps of cells, which may play a role in how the fungus infects people. In this study, we identified two different types of aggregation in *C. auris*, one triggered by antifungal treatment, and another controlled by growth conditions. This discovery allowed us to study aggregate formation in the same genetic background. In doing so, we found that a certain protein, an ALS-family adhesin, is involved in the aggregation process. Surprisingly, we also discovered that aggregates may promote infection by making it harder for the immune system to clear the yeast. This new understanding could help researchers develop better ways to fight *C. auris* infections.

67 ## Introduction

68 The fungus *Candida auris*, first identified in 2009, has been responsible for outbreaks of
69 infections in hospitals on six continents [1,2]. It has become a global concern due to the
70 high levels of antifungal resistance displayed across the species, its environmental
71 persistence, and its nosocomial transmission [3,4]. The species is divided into 5 clades
72 which have distinct geographic origins and show different levels of intra-clade variations.
73 The 4 main clades, clade I (South Asia), clade II (East Asia), clade III (South Africa), and
74 clade IV (South America) are well documented, whereas only a few isolates of clade V
75 (Iran) have been identified so far [5–7].

76 In fungi, morphological changes have been linked to gene expression modifications that
77 can impact virulence and pathogenicity [8,9]. For example, the expression of adhesins
78 and proteases are co-regulated alongside the yeast-to-hyphae transition of *Candida*
79 *albicans* [10]. The yeast *C. auris* typically grows as single ellipsoidal cells, and can form
80 filaments, but not true hyphae, under certain conditions [11,12]. Furthermore, certain *C.*
81 *auris* strains can form aggregates, which are clumps of cells that cannot be dispersed by
82 chemical or mechanical means and that are thought to be caused by a cell separation
83 defect [13–15]. Cellular aggregation is a phenotype predominantly of clade III strains, but
84 there are also aggregative isolates in clade I and clade II [16–18]. The biological
85 relevance and the genetic requirements for this aggregation morphology are not fully
86 understood yet [19], but some potential factors have recently been identified
87 [14,17,20,21]. Indeed, this kind of cellular behaviour can also be observed in other
88 species of the *Candida haemulonii* complex [21], to which *C. auris* belongs. *C. auris*
89 strains displaying the aggregation phenotype seem to be less virulent, more commonly

90 associated with skin colonisation, have greater biofilm mass, and greater environmental
91 persistence over non-aggregative isolates [16,18,22,23]. A recent study has distinguished
92 two types of aggregation, and has suggested that overexpression of an ALS-family
93 adhesin, caused by copy-number variation of the corresponding locus, is involved in this
94 [17]. So far, a major limitation of studies exploring aggregation has been that aggregative
95 strains are often compared to non-aggregative ones from different clades.

96 Our study has revealed that there are two different kinds of aggregation both of which
97 represent an inducible phenotype. One type of aggregation depends on growth conditions
98 and can only be induced in aggregative strains (mostly clade III strains). The other
99 depends on treatment with sub-inhibitory concentrations of echinocandins (a class of
100 antifungal drugs) and can also be induced in non-aggregative strains. The first type of
101 aggregation is induced by growth in rich medium and repressed in minimal medium. In
102 contrast to media-induced aggregates which are seemingly caused by cells sticking to
103 each other, echinocandin-induced aggregation is characterized by cells that fail to fully
104 separate [15]. Having identified the conditions for media-induced aggregation, we
105 exploited this to elucidate the genetic requirements for this type of aggregation. For this,
106 we performed transcriptomic analysis to identify differentially expressed genes in
107 aggregative and non-aggregative strains grown in rich and minimal medium. We identified
108 a gene with homology to a *C. albicans ALS* gene that is strongly upregulated in the
109 aggregative strain when grown in rich medium. We constructed a deletion mutant of this
110 gene, and the resulting strain lacks the ability to aggregate in rich medium, but still
111 aggregates in response to sub-inhibitory concentrations of echinocandins. We also show
112 that virulence in an invertebrate infection model is affected by pre-infection culture

113 conditions especially for strains with moderate or low virulence. If aggregation is
114 prevented by deletion of the upregulated ALS factor in an aggregative strain, then
115 virulence is moderately reduced. Finally, we used macrophages derived from
116 THP-1 monocytes to demonstrate that aggregates could be difficult for the immune
117 system to clear, and thus could potentially be responsible for persistent infections.

118

119 Results

120 Two distinct types of aggregation

121 The ability to aggregate (or not) has been used to classify strains of *C. auris*, and several
122 studies have reported aggregative capacities for some clinical isolates [15,18,24]. It was
123 thus surprising that, when grown in RPMI-1640, a defined minimal medium, we observed
124 a lack of this phenotype regardless of clade or status as aggregative or non-aggregative
125 strain (Fig 1A). However, we did observe that, if grown in Sabouraud dextrose broth
126 (SabDex), an undefined rich medium, the clade III strain (UACa20) and the clade IV strain
127 (UACa22) did form aggregates alongside single yeast cells, whereas non-aggregative
128 clade I (UACa11) and clade II (UACa83) strains did not show any clumping of cells (Fig
129 1A). The inability of this clade I isolate to aggregate, as well as the aggregative ability of
130 the clade III strain, we used in this study, agreed with previous observations [16].

131 We also found that, after growth in SabDex, aggregation was affected by the chemical
132 composition of the liquid used to resuspend the cells. Aggregating cultures retained
133 aggregation when resuspended in 1× PBS (phosphate-buffered saline), but aggregation
134 was greatly reduced when cells were resuspended in ddH_2O (Fig 1B). Interestingly, cells

135 that were dis-aggregated in ddH_2O, immediately re-aggregated when they were then
136 resuspended in 1× PBS (Fig 1B). Non-aggregative strains remained as single cells
137 regardless of suspension liquid (Fig 1B). This strongly indicates that a cell wall component
138 that remains present regardless of the change in suspension liquid is associated with
139 aggregation.

140 It has been reported that *C. auris* strains aggregate in response to sub-inhibitory
141 concentrations of two classes of antifungals, azoles, and echinocandins [15,16]. We
142 focused on two echinocandins, caspofungin (CSP) and micafungin (MFG) as these drugs
143 are used preferentially in the clinical setting to treat *C. auris* infections (CDC Guidelines,
144 PHE Guidlines). E-test strips were used to determine minimum inhibitory concentrations
145 (MICs) for the strains tested (Table S1). Growth was not completely abolished at any
146 concentration of CSP but was clearly diminished above a certain concentration which we
147 recorded as the MIC_{90} value (Table S1, Fig S1). Growth in the presence of MFG was
148 abolished above 0.094 mg/L for clade I strains UACa11 and UACa25 (Table S1, Fig S2).
149 However, for the clade III strains (UACa10 and UACa20) MIC_{90}s of 0.094 mg/L and 0.064
150 mg/L, respectively, were determined as residual background growth was observed above
151 these concentrations (Table S1, Fig S2). Therefore, 32 mg/L CSP and 0.075 mg/L MFG
152 were chosen as subinhibitory concentrations.

153 Echinocandin-induced aggregation experiments were performed in RPMI-1640 to avoid
154 clade III strains forming media-induced aggregates. Indeed, both the aggregative clade
155 III strain (UACa20) and the non-aggregative clade I strain (UACa11) formed aggregates
156 when grown in RPMI-1640 containing either 32mg/L CSP or 0.075 mg/L MFG (Fig 2A-B),
157 but not in the presence of the DMSO vehicle (Fig S3). These aggregates did not disperse

158 when cells were resuspended in ddH_2O, indicating that antifungal-induced aggregation
159 differs from media-induced aggregation (Figs 1B, 2A-B). This difference was also
160 noticeable when looking at the liquid cultures. After 5 minutes without agitation there was
161 noticeable sedimentation of the media-induced aggregates in the aggregative UACa20
162 (clade III) strain not seen in any of the other cultures (Fig 2C). However, both the non-
163 aggregative UACa11 (clade I) isolate and the aggregative UACa20 (clade III) strain
164 largely remained in suspension when echinocandin-dependent aggregates were formed
165 (Fig 2C). Neither media- nor echinocandin-induced aggregation was reflected in an
166 altered colony morphology on solid medium (Fig 2D).

167 The capacity of media-induced aggregates to dissociate and reform depending on the
168 suspension liquid, suggests the involvement of a component of (or associated with) the
169 cell wall, whereas the stability of antifungal-induced aggregates is consistent with a cell
170 separation defect [15]. To explore these phenotypes in more detail, we used calcofluor
171 white (CFW) to stain total cell wall chitin on paraformaldehyde-fixed cells. Media-induced
172 aggregates contained a mix of larger rounded cells marked with multiple bud scars
173 alongside smaller ellipsoidal cells (Fig 3A). It was also noted that the media-induced
174 aggregates started to fall apart when proteinase K treatment was used during preparation,
175 causing aggregates to spread out across glass slides during preparation for microscopy.
176 No pressure was applied during preparation as a hard-set mounting medium was used.
177 In contrast, echinocandin-induced aggregates appeared to grow from a small cluster of
178 cells with daughter cells emanating from a central point (Fig 3B). These tight clusters of
179 cells retained their shape during microscopy even after treatment with proteinase K. The
180 daughter cells appeared to remain attached to their mothers indicating a cytokinesis

181 defect similar to rapamycin-treated cells [25]. A lack of obvious bud scars on cells at the
182 edge of clusters corroborates this interpretation (Fig 3B) [25].

183 To better understand whether antifungal-induced aggregation was due to a cell
184 separation defect, confocal microscopy was used to visualize aggregates in three
185 dimensions. UACa20 (clade III) cells grown in SabDex were double-stained with CFW
186 (chitin) and Concanavalin A (ConA) (cell wall mannan). Media-induced aggregates
187 displayed an intact chitin cell wall that was completely covered by mannan (Fig 3C, red
188 arrows). Only small budding cells lacked the mannan outer cell wall layer between mother
189 and daughter cells (Fig 3C, white arrows). In contrast, cells in antifungal-induced
190 aggregates had a chitin layer completely surrounding them, but there was a lack of a
191 mannan layer where cells were closely juxtaposed (Fig 3D, white arrows), similar to small
192 budding cells in media-induced aggregates. Again, this is consistent with the idea that
193 antifungal-induced aggregation is the result of a cell separation defect, as previously
194 suggested [13–15,17].

195 During the preparation of cells for microscopy we noted that there was a lack of cohesion
196 of media-induced aggregates as well as loss of aggregation after treatment with
197 proteinase K for 1 hour at 50 °C. This was never observed for echinocandin-induced
198 aggregates. To quantify this observation, aggregates were counted using a
199 haemocytometer, and 1×10^6 aggregates were heated at 50 °C for 1 hour with or without
200 12.5 μg of proteinase K. The $\log_2$-fold change of aggregates remaining after treatment
201 was determined relative to number of aggregates before treatment. As predicted, the
202 number of media-induced aggregates showed a significant decrease when proteinase K
203 was present. For UACa20 (clade III), there was a significant ~15-fold decrease ($p = 0.03$,

204 independent samples t-test), and UACa10 (clade III) showed a significant ~28-fold
205 decrease ($p < 0.001$, independent samples t-test) in aggregates after treatment with
206 proteinase K (Fig 4A). These results are consistent with observations by others [17,21],
207 and suggest that the cell wall component involved in media-induced aggregation is not
208 perturbed by temperatures up to 50 °C. Neither CSP- nor MFG-induced aggregates were
209 significantly reduced by proteinase K treatment (Fig 4B-C).

210 Based on these observations, to semantically distinguish these phenotypes, we propose
211 that media-induced aggregation is henceforth referred to as "aggregation", whereas
212 aggregation caused by a cell separation defect is called "clustering". We focused on
213 aggregation induced by growth conditions to understand why this phenotype only occurs
214 in some isolates of *C. auris* and what the biological relevance of this phenotype might be.

215 **Media-induced aggregation is not correlated with cell wall ultrastructure**

216 Dispersion of aggregates by proteinase K suggested that a proteinaceous cell wall
217 component is involved in media-induced aggregation. To rule out other cell wall
218 ultrastructure changes and a potentially obscure cell separation defect, transmission
219 electron microscopy (TEM) was performed. Cells were grown in either RPMI-1640 or
220 SabDex before high-pressure freezing fixation without washing. No noticeable differences
221 in the cell wall ultra-structure were observed between conditions for all strains regardless
222 of the growth conditions (Fig 5A).

223 The diameters of the inner and outer cell walls for 30 cells from each condition were
224 measured. The diameter of the inner cell wall of non-aggregative strain UACa25 (clade I)
225 showed a significant increase of 21 nm ($p < 0.001$, independent samples t-test) when
226 grown in SabDex compared to RPMI-1640, but there was no significant difference for

227 UACa11 (clade I), a second non-aggregative strain. Aggregative clade III strains UACa6
228 and UACa20 grown in SabDex had significantly thicker inner cell walls by 20 nm ($p <$
229 0.001, independent samples t-test) and 25 nm ($p < 0.001$ independent samples t-test),
230 respectively, than when grown in RPMI-1640 (Fig 5A). The mannan fibrils (outer cell wall)
231 of UACa25 (clade I) were significantly longer by 18 nm ($p < 0.001$, independent samples
232 t-test) when grown in SabDex compared to RPMI-1640 (Fig 5B). While UACa20 (clade
233 III) grown in SabDex had slightly longer mannan fibrils by 4 nm ($p = 0.029$, independent
234 samples t-test) compared to when grown RPMI-1640. There were no significant
235 differences of outer cell wall diameters for UACa6 (clade III) and UACa11 (clade I).
236 Although there were differences in inner and outer cell wall thickness between the two
237 growth conditions, there was no clear trend which separated aggregative from non-
238 aggregative isolates.

239 **Transcriptomic analysis identifies clade-specific and aggregation-specific**
240 **differentially expressed genes**

241 We had shown that the aggregation phenotype is inducible in aggregative isolates, which
242 mostly belong to clade III (Fig 1A). Therefore, we opted to exploit this by using RNA-seq
243 to characterize genetic requirements and identify drivers of aggregation in UACa20 (clade
244 III) compared to the non-aggregative clade I strain UACa11. We compared differentially
245 expressed genes (DEGs) between growth in RPMI-1640 and SabDex for both strains,
246 and then compared these DEGs between UACa20 (clade III) and UACa11 (clade I) to
247 identify changes in transcription that may be important for aggregation. Differential
248 expression analysis was carried out by pairwise comparison between each sample group
249 each consisting of three independent samples, which allowed identification of DEGs

250 between growth in SabDex compared to RPMI-1640 with genes being identified from the
251 *C. auris* B11221 genome (UACa20 in this study). For UACa11 (clade I), from a total of
252 5,419 candidate open reading frames 3,191 significant DEGs at FDR < 0.05 were
253 identified (Fig 6A). For UACa20 (clade III), from a total of 5,431 candidates 3,393
254 significant DEGs at FDR < 0.05 were determined (Fig 6B). There were 997 common
255 DEGs between the two strains. These genes may be involved in adapting to growth under
256 the two different media conditions (Fig 6C), and hence were excluded from further
257 analysis. Genes with a log2FC difference greater than 2 between UACa20 (clade III) and
258 UACa11 (clade I) but with increased expression in SabDex in both strains were identified
259 (Table S2). Furthermore, we also extracted genes that displayed expression in opposite
260 directions between UACa11 (clade I) and UACa20 (clade III) when grown in SabDex
261 (Table S3). Ultimately, we decided to focus on genes that were uniquely upregulated in
262 the aggregative UACa20 strain compared to the non-aggregative UACa11 strain during
263 growth in SabDex, as we hypothesized that this would lead us to a positive effector of
264 aggregation. UACa11 (clade I) had 505 unique DEGs during growth in SabDex, while
265 UACa20 (clade III) had 658 unique DEGs (Fig 6C).

266 The top 10 unique genes upregulated during SabDex growth for UACa11 (clade I) and
267 UACa20 (clade III) are shown in Tables S4 and S5, respectively. To understand their
268 possible gene functions the *C. albicans* homologues were identified. First, the B11221
269 nucleotide sequence of each of those genes (Tables S4-S5) was BLAST-searched
270 against the B8441 genome and the corresponding gene/systematic ID names in B8441
271 were obtained. The B8441 gene identifiers were then used in the batch-download feature
272 of the *Candida* genome database (http://www.candidagenome.org) to identify

273 orthologues and best hits in the *C. albicans* SC5314 genome. The best hit in UACa11
274 (clade I) (Table S4) and the second-best hit in UACa20 (clade III) (Table S4) have been
275 identified as homologous to *C. albicans ALS4*. However, these represent two different *C.*
276 *auris* genes and they show differential regulation in regard to growth media, which was
277 unexpected. ALS (Agglutinin-Like Sequence)-containing proteins form a family of nine
278 adhesins in *C. albicans* with various roles including adherence to plastic and host tissues
279 [26]. *C. auris* genomes seem to contain three separate loci that harbour an Agglutinin-
280 Like Sequence (ALS) [27,28]. Representatives from clade II miss one of the *ALS*-family
281 genes, and in some strains a particular *ALS* gene might be amplified (copy-number
282 variation) [17,28]. Intriguingly, one of these factors (B9J08_004112, XP_028889036) has
283 mostly been studied, and varyingly touted as the ortholog to *C. albicans* Als3 [29], Als4
284 [17,28], or Als5 [22]. This is confusing, and as ALS factors in *C. albicans* have distinct
285 roles and different expression patterns, it is imprudent to assign orthology in *C. auris* when
286 function and gene expression cues have not been established in this species. Indeed,
287 phylogenetic analysis indicates that ALS-family members cluster by species and not by a
288 particular type of ALS from different species [28], this also seems to be the case for Hyr/Iff-
289 like adhesins [30]. To prevent further confusion, we follow the solution proposed by
290 O'Meara and colleagues [31] to use the unique number in the systematic ID as gene
291 number. And therefore, B9J08_004112/XP_028889036 should be called Agglutinin-Like
292 Sequence 4112 (*ALS4112*/Als4112), B9J08_002582 *ALS2582*, and B9J08_004498
293 *ALS4498*. This nomenclature should avoid potential confusion with ALS-type proteins
294 from other species where exact relationships are hard to establish.

295 **Als4112 is necessary for aggregation**

296 The *C. albicans* ALS-family proteins are found on the cell surface, play prominent roles
297 in adhesion to host tissues and other surfaces, and are important for virulence [26,32,33].
298 As media-induced aggregation is likely caused by a cell surface protein and *ALS4112*
299 displays differential expression during SabDex and aggregative growth in UACa20 (clade
300 III), this gene was taken forward as a candidate for potentially playing a role in
301 aggregation. We attempted to generate a clean *als4112* deletion in the aggregative strain
302 UACa20 (clade III). Unfortunately, due to the difficulties in the genetic manipulation of *C.*
303 *auris* [12,19,34], the one mutant strain we obtained harboured an approximate 21.3 kb
304 deletion encompassing the *ALS4112* locus and genes CJI97_004175, CJI97_004176,
305 CJI97_004177, CJI97_004178, CJI97_004179, CJI97_004180, as determined by inverse
306 PCR (Fig S4). We proceeded with this mutant as the additional genes deleted were not
307 present as DEGs in our RNA-seq dataset and are, therefore, not thought to play a role in
308 aggregation; the *als4112* mutant strain also did not display an obvious growth defect. This
309 *als4112* mutant failed to aggregate after 24 hours of growth in SabDex but did still cluster
310 upon exposure to 0.075 mg/L MFG (Fig 7A). This reinforces the idea that there are two
311 distinct types of aggregation, because the same type of cell separation defect is observed
312 in echinocandin-induced clustering in the wild-type clade III UACa20 strain, as well as in
313 the *als4112* mutant made in the same background (Figs 3D and 7B). Thus, *ALS4112*
314 appears to be a key genetic requirement for media-induced aggregation but not for
315 echinocandin-mediated clustering.

316 **Virulence depends on growth conditions of cells before inoculation**

317 There are mixed reports regarding the impact of aggregation on virulence in *Galleria*
318 *mellonella* and mouse infection models, with some studies showing reduced virulence of
319 aggregative strains in contrast to others observing no such a correlation [13,18,35].
320 Indeed, an infection study conducted in neutropenic mice found that there was no obvious
321 association of a given strain's virulence with either its aggregative capacity or it being
322 isolated from the blood stream [18]. Given that in other *Candida* species, such as *C.*
323 *albicans*, virulence can be influenced by cellular morphology [10], we decided to
324 investigate whether virulence was impacted by the aggregation morphology or was
325 isolate-dependent using an *in vivo G. mellonella* infection assay. Fungal cells were grown
326 in either RPMI-1640 as single cells or pre-grown in SabDex inducing the aggregation
327 phenotype in aggregative isolates UACa20 (clade III), UACa6 (clade III), and UACa23
328 (clade IV) while non-aggregative isolates UACa11 (clade I), UACa25 (clade I), and
329 UACa83 (clade II) remained as single cells, before being injected into the moth larvae.

330 All isolates, with the exception of UACa25 (clade I), showed a significant ($p < 0.05$)
331 increase in killing regardless of their ability to aggregate when grown in SabDex, rather
332 than RPMI-1640, before inoculation (Fig 8A-F). This suggests that virulence does not
333 depend directly on the ability to aggregate, but is more likely driven by more complex
334 strain-specific traits influenced by pre-inoculation culture conditions. Being grown in rich
335 medium (SabDex) before inoculation in particular boosts pathogenicity of strains with low
336 to moderate virulence (Fig 8C-F), whereas the two clade I strains receive comparatively
337 little benefit (Fig 8A-B). Indeed, also in *C. albicans* growth conditions influence virulence
338 in invertebrate and vertebrate models of infection [36,37].

339 As the *als4112* deletion strain in the UACa20 background allowed us to directly assess
340 whether aggregation impacts virulence. We also compared the wild-type UACa20 isolate
341 with UACa177 in the *Galleria* infection model after growing these strains in SabDex,
342 where UACa20 aggregates and UACa177 does not. The aggregating wild-type UACa20
343 isolate was moderately, but significantly, more virulent than the non-aggregating
344 *als4112*Δ mutant strain UACa177 (Figs 8G). This suggests that ALS-dependent
345 aggregation has a positive effect on virulence rather than a negative one as previously
346 thought [13].

347 **Aggregates are not cleared by macrophages**

348 Aggregates have been reported in tissue from sacrificed animals [18]. Given the bulky
349 nature of aggregates, we wanted to understand how they would interact with
350 macrophages. THP-1 monocytes were differentiated into macrophages with 200 nM
351 phorbol 12-myristate 13-acetate (PMA) and co-cultured at a multiplicity of infection (MOI)
352 of 1:3 with UACa20 (clade III) cells, which were either grown in SabDex, RPMI-1640,
353 RPMI-1640 containing 0.001% DMSO, or RPMI-1640 containing 0.075 mg/L MFG and
354 0.001% DMSO. Cells were washed and added to CO_2-independent medium for co-
355 culture. Aggregates were counted as one unit for MOI; because cell uptake by
356 macrophages was not quantified, we do not consider this an issue. For cells grown in
357 RPMI-1640 or RPMI-1640 containing 0.001% DMSO, there was no noticeable defect in
358 uptake of single yeast cells (Videos V1 & V2). When presented with media-induced
359 aggregates (Fig 9A, Video V3) or MFG induced clusters (Fig 9B, Video V4) macrophages
360 struggled to engulf the mass of fungal cells with fungal growth occurring at the site not
361 occupied by the macrophage. Media-induced aggregation is not complete, as it produces

362 a heterogenous population of single cells and large aggregates. The single yeast cells
363 under these co-culture conditions are readily taken up by macrophages (Video V5). This
364 indicates that there is no issue with sensing the *C. auris* cells growing under aggregating
365 conditions but that the ability of macrophages to clear the fungal aggregates is dampened.
366 Aggregation and clustering could potentially be causes for long-term persistence of fungal
367 cells in the host and thereby contribute to increased virulence.

368

369 **Discussion**

370 Here, we show that aggregative *C. auris* strains, usually belonging to clade III, only
371 aggregate when grown in a rich medium, such as SabDex or YPD (Fig 1A). This
372 aggregation phenotype is repressed in a minimal medium, such as RPMI-1640, in which
373 aggregative strains grow as single-celled yeasts, like non-aggregative strains (Fig 1A). A
374 second type of aggregation, which we suggest calling “clustering”, was seen when cells
375 were exposed to sub-inhibitory concentrations of echinocandins. This clustering can be
376 induced in aggregative and non-aggregative strains (Fig 2). Such changes in
377 morphological phenotype in *C. auris,* which are triggered by environmental cues, are likely
378 biologically relevant. Similar morphological transitions are observed in other *Candida*
379 species where the switches are often associated with cell stress, such as increased
380 temperature or lack of nutrients [38,39]. SabDex is a rich undefined medium, so the switch
381 of aggregative strains to grow as aggregates suggests that either rich medium is causing
382 some cellular stress or contains specific chemical triggers for such a switch. Indeed, our
383 work highlights the importance of selecting appropriate growth conditions for
384 experimentation with *C. auris,* especially when the aggregation phenotype is to be

385 dissected. Hence, publicly available data from previous work should be reanalysed
386 cautiously [15], as effects of media-induced aggregation and antifungal-induced
387 clustering could potentially confound each other.

388 It was originally assumed that aggregates in *C. auris* formed due to a lack of cell
389 separation [13]. Indeed, some genetic requirements for this type of cell clustering have
390 been identified by elegant forward genetic screening [14,40]. We only saw this particular
391 phenotype when we exposed *C. auris* strains to echinocandins, and this did not happen
392 when *C. auris* clade III strains were grown in rich media (Fig 1A & 3). However, Bing *et*
393 *al*. (2023) characterized a clinical *C. auris* clade I isolate that forms clusters via a cell
394 separation defect, which seems to be inherent to this particular strain [17]. It will be
395 interesting to assess whether clustering in this strain can be modulated by growth
396 condition or is exacerbated by treatment with echinocandins. In the same study [17], a *C.*
397 *auris* clade III strain was shown to undergo proteinase-sensitive aggregation which is
398 associated with overexpression of an ALS-type adhesin (B9J08_004112). For reasons
399 outlined above, we refer to B9J08_004112 as *ALS4112*. Overexpression of Als4112 (Bing
400 *et al*. call it Als4 [17]) in some clinical *C.auris* clade III isolates is apparently caused by
401 copy-number variation of that gene apparently linked to adherence and biofilm forming
402 capability [17]. Copy-number variation and induced gene expression levels also neatly
403 explain our observation that a change in media provokes aggregation. In such a scenario,
404 an aggregative strain expresses Als4112 at low levels when grown in minimal medium
405 (RPMI-1640) but has a high-enough copy number of *ALS4112* [17] to produce sufficient
406 protein molecules to enable aggregation once expression is induced. Here, we find that
407 the non-aggregative UACa11 clade I strain does not upregulate expression of *ALS4112*

408 when grown in SabDex but a different *ALS* gene, *ALS2582* (B9J08_002582). Als2582 at
409 861 amino acids is considerably smaller than Als4112 (1804 amino acids). Our data
410 suggest that Als2582 does not drive aggregation, as UACa11 (clade I) does not form
411 aggregates. Whether this particular adhesin is involved in biofilm formation, adherence to
412 host cells, or adherence to other surfaces (medical equipment) remains to be tested.
413 Indeed, a recently identified *C. auris*-specific adhesin, Scf1, contributes to virulence by
414 promoting adhesion to both biological and abiotic surfaces [31].

415 We show that antifungal treatment causes a cell separation defect which leads to the
416 formation of cell clusters, and that this phenotype is independent of the ability to
417 aggregate in response to the growth media, which has been assumed to be the typical
418 aggregation phenotype [13,17]. Although this is an important distinction to make, both
419 forms of aggregation are apparently hard to clear by the immune system, as our
420 coincubation experiments with macrophages show (Fig 9, Videos V1-V5). Further studies
421 will be needed to fully understand the implications of media-induced aggregation and
422 antifungal-mediated clustering on clinical treatment. The differences in aggregation types
423 might also explain the varying results linking biofilm formation and aggregation ability in
424 separate studies [17,22,23].

425 We focused our attention on media-induced aggregation as there is mounting evidence
426 that aggregation of this type is associated with increased biofilm formation and adherence
427 [17]. Given the importance of the cell wall in cell-cell interactions we examined the cell
428 wall ultrastructure comparing *C. auris* cells from different strains grown in RPMI-1640 and
429 SabDex (Fig 5). TEM showed a lack of obvious differences indicating that cell wall
430 mannans are not notably remodelled between aggregated and single cells, supporting

431 the hypothesis of a protein which is not a bulk component of the cell wall mediating media-
432 induced aggregation. We observed moderate, but significant differences in inner cell wall
433 thickness and mannan fibril length between growth condition in some isolates, but these
434 were strain-specific and not associated with a particular clade or the ability to aggregate.

435 Transcriptomic analysis demonstrated large differences in gene expression between
436 strains of different clades, with 505 DEGs unique to UACa11 (clade I) and 653 DEGs
437 unique to UACa20 (clade III). Of interest to us was that two distinct *ALS* genes were
438 differentially expressed indicating that different ALS-type adhesins might have separate
439 roles [16]. We produced an *als4112* null mutant with some difficulty despite trying multiple
440 techniques, including CRISPR-Cas9-targeted mutation [14]; this might have been
441 aggravated by copy-number variation at the locus [17]. Our *als4112* mutant unfortunately
442 is not a clean deletion, but the region removed does not contain differentially expressed
443 genes identified in our RNA-seq data (Fig S4). Therefore, these genes may not play a
444 role in aggregation and this mutant was thus used for analysis. The results suggest that
445 Als4112 is involved in media-induced aggregation as *als4112* cells formed no aggregates
446 after 24 hours of growth in SabDex. A different mechanism underpins antifungal-induced
447 clustering, as this phenotype was unaffected in *als4112*Δ cells (Figs 2 & 7). This result
448 corroborates the work by Bing *et al.* (2003) where they showed that overexpression of
449 Als4112 induced the aggregation phenotype in non-aggregating strains and that clinical
450 isolates lacking a fully functional Als4112 do not aggregate [17].

451 The *G. mellonella* infection model has been useful for comparing the pathogenicity of *C.*
452 *auris* strains [35]. Intriguingly, we show that the choice of growth medium for the inoculum
453 has a significant impact on the outcome (Fig 8A-F). Cells grown in SabDex are more

454 virulent than those grown in RPMI-1640 for all strains tested except one, the non-
455 aggregative clade I strain UACa25. Further testing with a lower starting inoculum of
456 UACa25 (clade I) would rule out a toxic shock phenomenon that could be caused by
457 UACa25 (clade I) having a higher overall virulence compared to other strains (Fig 8A-F).
458 This demonstrates the importance of experimental design and of detailed reporting of
459 experimental conditions to enable a valid comparison across published results.
460 Importantly, when the contribution of aggregation to virulence was directly tested by
461 comparing the wild-type UACa20 isolate to the *als4112*Δ mutant, wild-type infection
462 reduced survival among *G. mellonella* larvae significantly (Fig 8G).

463 Another difficulty working with aggregation is to correctly determine the number of cells
464 without removing the aggregates from the cell culture before inoculating a host.
465 Therefore, we analysed host-pathogen interaction using macrophages to elucidate how
466 the immune system might deal with *C. auris*. We observed that the uptake of single yeast
467 cells was not impeded in a noticeable way even if aggregates were present (Video V5).
468 Interestingly, macrophages interacted with aggregates but were unable to fully engulf or
469 clear them (Fig 9, Videos V1-V5). We also observed that many macrophages ignored
470 fungal cells which is in line with previous observations [41]. The inability of the immune
471 system to clear aggregates would explain their presence in animal models post infection
472 [18]. We hypothesize that cell aggregates might act as reservoirs in the host during
473 infection, with single cells being cleared by resident macrophages during active infection.
474 However, aggregates might persist for longer times, and cause breakthrough infections
475 when the immune system of the host is weakened or suppressed. Whether this explains
476 the higher virulence of an aggregative wild-type strain compared to a non-aggregative

477 *als4112* mutant requires further experimentation with primary human macrophages and
478 a whole-animal mammalian infection model.

479 To summarize, we have shown that there are two types of aggregation, canonical strain-
480 inherent aggregation induced by the growth environment, and a different morphology we
481 call “clustering” which is mediated by sub-inhibitory concentrations of echinocandins. We
482 have demonstrated that an ALS-family adhesin, Als4112, is involved in media-induced
483 aggregation, and that aggregates of both types pose a challenge for the immune system
484 and might be a cause of the persistence of *C. auris* systemic infections.

485

486 Materials & Methods

487 Yeast strains and culture conditions

488 All strains used in the study are listed in Table S6. All strains were recovered from storage
489 at -70 °C, grown for 1 day at 37 °C and maintained for up to 1 month on mycological YPD
490 (1% yeast extract (Oxoid Ltd., Basingstoke, UK), 2% mycological peptone (Oxoid Ltd.),
491 2% D-glucose (Thermo Fisher Scientific, Waltham, MA, USA) and 2% agar (Oxoid Ltd.))
492 slopes at 4 °C, with fresh cultures spread on mycological YPD plates and incubated at 37
493 °C for 2 days before use. All experiments were performed in Sabouraud dextrose
494 (SabDex) (1% mycological peptone (Oxoid Ltd.), 4% D-glucose (Thermo Fisher
495 Scientific)) or RPMI-1640 (10.4 g/L RPMI-1640 powder without phenol red (Merck KGaA,
496 Darmstadt, Germany), 1.8% D-Glucose (Thermo Fisher Scientific), 0.165 M 3-(N-
497 morpholino)propanesulfonic acid (Melford, Suffolk, UK) adjusted to pH 7 by 1 M NaOH
498 (Sigma-Aldrich, Burlington, MA, USA)). Cultures were grown at 37 °C shaking at 200 rpm.

499 Where plates have been used it is the medium specified with the addition of 2% agar
500 (Becton, Dickinson & Co., Franklin Lakes, NJ, USA).

501 The antifungal drugs, Caspofungin and Micafungin, were purchased from Merck KGaA
502 and resuspended in DMSO (Merck KGaA). For liquid culture they were added to RPMI-
503 1640 as prepared above at time of fungal inoculation. For agar plates, the antifungals
504 were added to RPMI-1640 with 2% agar after autoclaving and the media temperature had
505 cooled to 60 °C to avoid degradation of the antifungal activity.

506 **Determination of Aggregation**

507 Strains were grown for 16 hours at 37 °C shaking at 200 rpm. Cells were harvested by
508 centrifugation (2,500 ×*g*, 5 minutes) after which culture media was removed. Cells where
509 then resuspended in 1× phosphate buffer saline (1× PBS) or ddH_2O this was repeated
510 twice to completely remove growth media. Cells finally suspended in 1× PBS or ddH_2O
511 were vortexed for 1 minute before microscopic examination to check for presence of
512 aggregates.

513 **Microscopy**

514 For light microscopy cells were suspended in the indicated solution and 50 µL was added
515 to a glass slide before images were captured on a Zeiss Axioskop 20 microscope with a
516 Axiocam 105 Colour using Zen 2.3 software (version 2.3.69.10000).

517 For fluorescence microscopy, cells were fixed with 4% methanol-free paraformaldehyde
518 overnight, cells were harvested by centrifugation (2,000 ×*g*, 5 minutes) and resuspended
519 in 1× PBS, this was repeated twice to remove traces of paraformaldehyde.

520 For cell wall chitin, cells were incubated for 1 hour with 10 µg/mL Calcofluor White M2R
521 (CFW) (Merck KGaA). Cells were harvested by centrifugation (2,000 ×*g*, 5 min) and
522 supernatant removed. Cells were resuspended in 10 µL Vectashield HardSet Antifade
523 Mounting Medium (2B Scientific, Kidlington, UK), which was placed on a microscope
524 glass slide and coverslip placed on top without applying pressure. Images were captured
525 on a Zeiss Imager M2 upright microscope with a Hamamatsu Flash 4 LT camera using
526 Zen 2.3 software (version 2.3.69.1018).

527 For confocal fluorescent microscopy of chitin and mannan staining, fixed cells were
528 incubated with 1× PBS containing 1% bovine serum albumin (Merck KGaA) for 1 hour on
529 ice. This was removed by centrifugation (2,000 ×*g*, 5 min) and cells were resuspended in
530 1× PBS containing 10 µg/mL CFW and 25 mg/mL Concanavalin A (Con A) conjugated to
531 Alexa Fluor 488 for 1 hour on ice. Cells were harvested by centrifugation (2,000 ×*g*, 5
532 min) and resuspended in 1× PBS, this was repeated twice. After the final wash with 1×
533 PBS, cells were spun down again and supernatant was removed, cells were then re-
534 suspended in 10 µL Vectashield HardSet Antifade Mounting Medium and mounted onto
535 microscope slides, a coverslip was applied without pressure. Images were taken as Z-
536 stacks with an image every 0.1 µm with a Ultraview VoX spinning disk confocal
537 microscope using a Hamamatsu C11440-22C camera. Images were processed with
538 Volocity software (Version 6.5.1) selecting images that showed the connection point
539 between cells.

540 ***Galleria mellonella* survival assay**

541 Strains were prepared for inoculation by picking a single colony from a SabDex plate and
542 growing the cells for 16 hours in fresh liquid medium (SabDex or RPMI-1640). Medium

543 was removed by centrifugation (2,500 ×*g*, 5 minutes). Cells where then washed twice with
544 ddH_2O by centrifugation (2,500 ×*g*, 5 minutes) between each resuspension. Finally, cells
545 were suspended in 1× PBS. Cell suspensions stood for 10 minutes to allow aggregates
546 to sink to the bottom of the suspension and single cells were harvested from the top layer
547 of the solution for counting. Cells were adjusted to give a final inoculum of 50 µL
548 containing 5×10^5 cells in 1× PBS. *G. mellonella* larvae (TruLarv BioSystems
549 Technology, Exeter, UK or UK Waxworms Ltd, Sheffield, UK) were inoculated within two
550 days of receipt. A 50 µL inoculum was given via the last left proleg with a 0.5 ml 29G
551 Micro-Fine U-100 insulin injection unit (BD Medical, Franklin Lakes, NJ, USA).

552 Larvae were incubated for 6 days at 37 °C. Every 24 hours larvae were examined and
553 deemed dead when they no longer responded to physical stimuli. Each experiment also
554 had a non-injected control group and a control group injected with 1× PBS only. Results
555 were pooled across three independent experiments and statistical analysis was done
556 using a Kaplan-Meier survival plot followed by Log-rank test statistics to determine if
557 differences in survival were significant.

558 **MIC Testing**

559 Minimum inhibitory concentration (MIC) determination was done using Caspofungin and
560 Micafungin MIC E-test strips (Liofilchem srl, Roseto degli Abruzzi, Italy) following the
561 manufacturer's guidance with small modifications. Isolates were grown for 24 hours on
562 SabDex agar plates, one colony was picked and dispersed in ddH_2O. Onto RPMI-1640
563 agar plates 2×10^6 cells were spread and allowed to dry for 10 minutes. A MIC test strip
564 was carefully placed onto the agar surface, and the plate was incubated for 24 hours at
565 37 °C before determining the zone of inhibition and the MIC or MIC_{90} where appropriate.

566 **High-pressure freezing sample preparation for transmission electron microscopy**
567 **(TEM)**

568 Cells were grown for 16 hours in the indicated media. Cells were then harvested by
569 centrifugation (2,500 ×*g*, 5 minutes) and removal of excess cell culture media was
570 performed before fixation and preparation. Fixation and preparation were performed by
571 the Microscopy and Histology Core Facility at the University of Aberdeen following a
572 published protocol [42]. Fixation was done by high-pressure freezing using a Leica
573 Empact 2/RTS high-pressure freezer. Samples were returned to us and we performed
574 imaging using a JEOL 1400 plus transmission electron microscope with an AMT UltraVUE
575 camera. All images were processed, and cell wall thickness was measured with Fiji
576 (ImageJ version 1.53f51) [43].

577 **Proteinase K assay**

578 Cells were grown for 16 hours in the indicated liquid medium at 37 ˚C shaking at 200 rpm.
579 Cells were harvested by centrifugation (2,500 ×*g*, 5 minutes), the supernatant was
580 discarded before the pellet was resuspended in 1× PBS, centrifugation and resuspension
581 was repeated twice before aggregates were counted using a haemocytometer. For the
582 assay 1×10^6 cells were added to 50 µL of ddH_2O either containing 12.5 µg of proteinase
583 K or not before being incubated for 1 hour at 50 ˚C, a second ddH_2O sample was also
584 prepared and incubated at room temperature for 1 hour to ensure the application of heat
585 did not increase the number of aggregates. After incubation 950 µL 1× PBS was added,
586 and cells were vortexed at high speed for 1 minute. The number of aggregates were
587 counted again with a haemocytometer and the fold-change of aggregates between the

588 unincubated against the incubated samples calculated. Statistical significance was
589 determined by an independent samples t-test.

590 **Transcriptomics**

591 UACa20 (clade III) and UACa11 (clade I) were grown in the specified media for 16 hours
592 and RNA was extracted for RNA-sequencing (RNA-seq) using the method outlined below,
593 this was repeated three times on independent colonies at different times. After growth for
594 16 hours cells were harvested by centrifugation (2,500 ×*g*, 5 minutes). Supernatant was
595 discarded and cells resuspended in residual supernatant before immediately proceeding
596 to RNA extraction. RNA was extracted by homogenisation of cells with acid-washed glass
597 beads in 600 µL TRIazole (Invitrogen, Thermo Fisher Scientific, Waltham, MA, USA) per
598 60 µL culture using a FastPrep-24 5G (MP Biomedicals, Santa Ana, CA, USA) for cell
599 lysis. Glass beads and cell debris were discarded after centrifugation (12,000 ×*g* for 10
600 minutes at 4 °C) and the supernatant was used for further steps. Addition of 0.2 mL
601 chloroform per 1 mL TRIazole was followed by vigorous shaking for 15 seconds and
602 incubation at room temperature for 2 minutes. Centrifugation (12,000 ×*g* for 15 minutes
603 at 4°C) separated the proteins, DNA, and RNA into 3 phases. RNA in the aqueous layer
604 was removed and subjected to precipitation by addition of 500 µL isopropanol and
605 incubated at room temperature for 10 minutes. Centrifugation (12,000 ×*g* for 10 minutes
606 at 4°C) resulted in a pellet of RNA, which was washed with 600 µL 75% ethanol. Ethanol
607 was removed after centrifugation (6,000 ×*g* for 10 minutes at 4°C) and the RNA pellet
608 was dried for 10 minutes at room temperature. The RNA samples were resuspended in
609 RNase-free water before clean-up treatment with the RNase-Free DNase Set (Qiagen,
610 Hilden, Germany) following the manufacturer's protocol for off-column clean-up. RNA was

611 then subjected to further clean-up by using the RNeasy Mini Kit (Qiagen) following the
612 manufacturer's instructions, before final suspension in RNase-free water and storage at
613 -80 °C before sequencing.

614 Sequencing of mRNA was carried out by the Centre for Genome-Enabled Biology and
615 Medicine (CGEBM) at the University of Aberdeen. Before sequencing External RNA
616 Controls Consortium (ERCC) spike controls were added to samples for assessment of
617 library quality and as estimation of lowest limit of detection [44]. Library preparation was
618 done using Illumina TruSeq Stranded mRNA kit (Illumina Inc., San Diego, CA, USA) and
619 sequenced using the High Output 1×75 kit on the Illumina NextSeq 500 platform
620 producing 75 bp single-end reads. Quality control of the sequencing data was performed
621 using FastQC (version 0.11.8)
622 (https://www.bioinformatics.babraham.ac.uk/projects/fastqc/) with lower-quality reads
623 and adaptor content being removed with TrimGalore! (version 0.6.4)
624 (http://www.bioinformatics.babraham.ac.uk/projects/trim_galore/) with a Phred quality
625 score threshold of 30. ERCC spike controls consist of 92 synthesized transcripts that
626 range both in length and concentration. Two mixes (Mix 1 and Mix 2) are provided with
627 differing transcript concentration ratios of 4:1, 1:1, 1:1.5, and 2:1 to allow for assessment
628 of detection of differential expression. One of these two mixes was randomly added to
629 each of the samples. ERCC reads were removed by aligning all reads to the ERCC
630 reference genome using HISAT2 (version 2.1.0) [45] with unmapped *C. auris* reads being
631 kept for alignment. Illumina-sequencing produced between ~25 million and ~30 million
632 reads per sample (Table S7).

633 The *C. auris* B11221 reference genome was downloaded from NCBI
634 (https://www.ncbi.nlm.nih.gov/genome/38761?genome_assembly_id=678645) [46]
635 along with the equivalent annotation file and prepared for use with the alignment software
636 HISAT2 (version 2.1.0) [45]. Reads were aligned to this prepared reference using HISAT2
637 (version 2.1.0) [45] with the parameter for stranded library preparation used. SAMtools
638 (version 1.9) [47] was used to process the alignments and reads were counted at gene
639 locations using featureCounts (part of the sub-read version 1.6.2 package) [48] utilizing
640 the parameter to split multi-mapped reads as a fraction across all genes that they align
641 to, and the parameter for stranded analysis. 83.66% to 88.75% of reads aligned to coding
642 regions and after quality control and removal of low-count genes a total of 5,431 genes
643 remained for analysis.

644 edgeR (version 3.30.3) [49] was used to detect which genes had a significant differential
645 change in expression. All genes that had a CPM (count per million) value of more than
646 one in three or more samples were kept for analysis, and all other genes were removed
647 as low-count genes. Differential expression analysis was performed via pairwise
648 comparisons between each sample group. To obtain the B8441 gene names, the gene
649 DNA sequence for the B11221 strain was obtained and compared to the B8441 gene
650 sequences using BlastN [50].

651 ***als4112* mutant generation**

652 All genomic DNA was prepared as described previously [12]. All PCRs were done using
653 VeriFi Hot Start Mix (PCR Biosystems Ltd., London, UK), with the exception of
654 transformant screening which was done with PCRBIO Taq Mix Red (PCR Biosystems
655 Ltd.). The deletion mutant was generated by a previously described method of homology-

656 directed repair and lithium-acetate transformation [51] using a nourseothricin marker.
657 Briefly, the *CaNAT1* resistance marker was amplified from plasmid pALo218 using
658 primers oUA315 and oUA316 (Table S8) [12]. The *ALS4112* gene sequence and flanking
659 sequences 2 kb upstream and downstream were obtained from NCBI (Accession
660 XP_028889036.1) to design primers, 1 kb upstream and 1 kb downstream of *ALS4112*
661 was amplified with primers oUA989 and oUA990, and oUA991 and oUA992 respectively,
662 from UACa20 genomic DNA (Table S8). The deletion cassette was assembled using
663 fusion PCR and primers oUA993 and oUA994 (Table S8) to amplify the final deletion
664 cassette which was confirmed by gel electrophoresis. UACa20 (clade III) was grown
665 overnight at 30 ºC with shaking before being diluted 1:100 in fresh bacteriological YPD
666 (1% yeast extract (Oxoid Ltd.), 2% bacteriological peptone (Oxoid Ltd.), 2% D-glucose
667 (Thermo Fisher Scientific) and 2% agar (Oxoid Ltd.)) and grown for a further 4 hours.
668 Cells were then harvested by centrifugation for 2 minutes at 1,000 ×*g* and resuspended
669 in ddH_2O. This step was repeated twice before cells were suspended in 0.1 M lithium
670 acetate and were centrifuged again for 1 minute at 1,000 ×*g* before being suspended in
671 0.1 M lithium acetate. To this 5 µg of the deletion cassette in 50 µL of 50% PEG-3350, 1
672 M lithium acetate and 10 mg/mL denatured herring sperm DNA (Thermo Fisher Scientific)
673 was added and incubated overnight shaking at 30 ºC. Heat shock was applied in a heat
674 block the next day at 44 ºC for 15 minutes, and cells were resuspended in bacteriological
675 YPD and incubated shaking at 30 ºC for 3 hours to recover. After recovery cells were
676 plated on bacteriological YPD plates containing 200 µg/mL nourseothricin (clonNAT;
677 Werner BioAgents GmbH, Jena, Germany) and incubated at 30 ºC until colonies
678 appeared (usually 2 days). Transformants were screened for *als4112* deletion with

679 primers oUA987 and oUA988 (Table S8), and UACa20 genomic DNA was used as a
680 positive control.

681 **Inverse PCR**

682 Genomic DNA from the *als4112* null mutant was prepared as described previously [12].
683 Inverse PCR design is outlined in Fig S4. For the restriction digest 1 µg of genomic DNA
684 from UACa20 and *als4112*Δ was incubated for 1 hour at 37 ºC with the restriction
685 endonuclease BamHI-HF (New England Biolabs (NEB), Ipswich, MA, USA) following the
686 manufacturer's instructions. The enzyme was removed with the Monarch PCR & DNA
687 Cleanup Kit (NEB) following the manufacturer's instructions. For the ligation reaction 8 µL
688 of the digest was treated with T4 Ligase (NEB) for 16 hours at 16 ºC, before stopping the
689 reaction at 65 ºC for 10 minutes. PCR was done using VeriFi Hot Start Mix (PCR
690 Biosystems Ltd.) to amplify DNA for sequencing with primers oUA995 and oUA996 (Table
691 S8) for upstream region boundary of the deletion cassette and primers oUA997 and
692 oUA998 (Table S8) were used for the downstream boundary of the deletion cassette,
693 amplification of the *als4112*Δ DNA but not UACa20 DNA was confirmed by gel
694 electrophoresis. DNA was sent for Sanger sequencing (Eurofins Scientific, Luxembourg,
695 Luxembourg) with primers oUA999 for upstream and oUA1000 for downstream
696 sequencing (Table S8), and results were compared using BLAST against the *C. auris*
697 reference genome (NCBI Cand_auris_B11221_V1) to determine boundaries of the
698 deletion cassette.

699 **THP-1 Macrophage Differentiation**

700 The human monocyte cell line THP-1 (MerckKGaA) were maintained at 2×10^5 cells/mL
701 in RPMI-1640 containing 10% fetal bovine serum (FBS) (Thermo Fisher Scientific), 200

702 U/mL penicillin/streptomycin (Thermo Fisher Scientific), and 2 mM GlutaMAX (Thermo
703 Fisher Scientific) at 37 °C in 5% CO_2. Macrophages were differentiated with 200 nM
704 phorbol 12-myristate 13-acetate (PMA) (Merck KGaA) following a previously described
705 method with slight modifications [52]. Briefly 1 × 10^5 cells/ml were incubated in RPMI-
706 1640 with 200 nM PMA, 10% FBS, 200 U/mL penicillin/streptomycin, and 2 mM
707 GlutaMAX at 37 °C in 5% CO_2 for 3 days. PMA-containing media and non-adherent cells
708 were removed by washing twice with 1× PBS. THP-1 macrophages were then allowed to
709 rest for 3 days in RPMI-1640 with 10% FBS, 200 U/mL penicillin/streptomycin, and 2 mM
710 GlutaMAX at 37 °C in 5% CO_2. Media was removed and THP-1 macrophages were lifted
711 by scraping. 2 × 10^5 THP-1 macrophages were added to each well of an 18-well slide
712 (ibidi, Gräfelfing, Germany) in RPMI-1640 supplemented with 10% FBS, 200 U/mL
713 penicillin/streptomycin, and 2 mM GlutaMAX at 37 °C in 5% CO_2 and allowed to rest for
714 a further 24 hours before being used for experimentation.

715 **Live-Cell Imaging**

716 Fungal cells were grown for 24 hours in desired media and cells were harvested by
717 centrifugation 2,000 ×*g* for 5 minutes and resuspended in ddH_2O, this was repeated twice
718 before cells were counted with a haemocytometer. Medium was removed from THP-1
719 macrophages and replaced with CO_2-independent medium (Fisher Scientific) containing
720 fungal cells at MOI 1:3 and 0.02 µg/µL propidium iodide (Fisher Scientific). Images were
721 taken every 3 min for 2 hours on an Ultraview VoX spinning disk confocal microscope
722 using Volocity software (Version 6.5.1).

723 **Statistics**

724 All statistics were performed in SPSS Statistics for Windows (version 28.0) (IBM Corp.,
725 Armonk, NY, USA) except for log-rank tests of *G. mellonella* survival data which were
726 performed in R (version Rx64, 4.3.0) (http://www.r-project.org/).

727

728 **Acknowledgments**

729 We are grateful to Rhys Farrer (MRC CMM, University of Exeter) for guidance on
730 bioinformatic analysis, to Louise Walker (University of Aberdeen) for advice on
731 macrophage work, and to Neil A. R. Gow (MRC CMM, University of Exeter) and Dhara
732 Malavia (MRC CMM, University of Exeter) for discussing their unpublished results. We
733 thank Gillian Milne (Microscopy & Histology Facility, University of Aberdeen) for technical
734 assistance with electron microscopy. *Candida auris* strains were kindly provided by
735 Anuradha Chowdhary (Vallabhbhai Patel Chest Institute, University of Delhi, Delhi, India),
736 Public Health England (PHE) (Bristol, UK), and the Mycotic Diseases Branch of the
737 Centers for Disease Control and Prevention (CDC) (Atlanta, GA, USA).

738

739 **Funding**

740 This work was supported by a PhD studentship (MR/P501955/1) from the Medical
741 Research Council (MRC) Centre for Medical Mycology at the University of Exeter, UK
742 (MR/N006364/2). The funders had no role in study design, data collection and analysis,
743 decision to publish, or preparation of the manuscript.

744

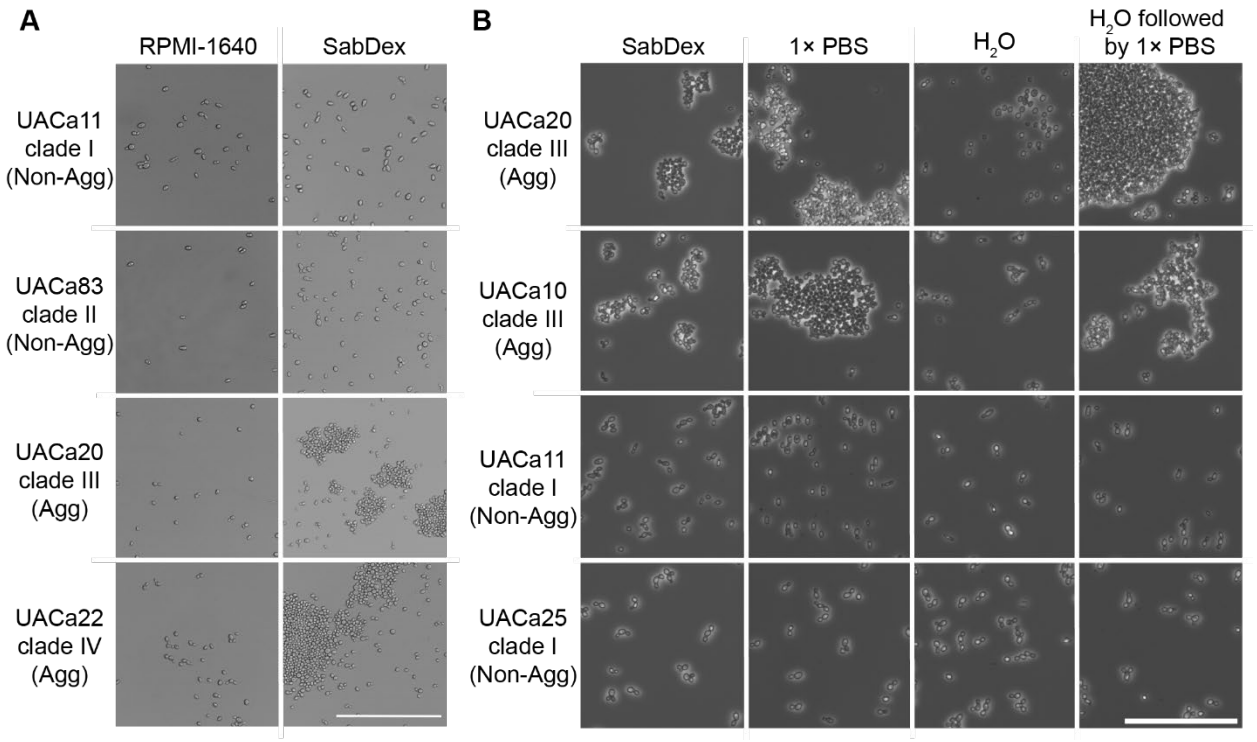

745

746 **Fig 1. Aggregation is an inducible phenotype.** (**A**) Changes in growth media induce
747 aggregation only in aggregative strains. Light microscopic (brightfield) images of cells of the
748 indicated strains (left) in the indicated medium (top). Cells grown in RPMI-1640 displayed no
749 aggregation regardless of ability to aggregate. Only aggregative (Agg) strains grew as aggregates
750 when grown in SabDex while non-aggregative (Non-Agg) strains remained as single cells. (**B**)
751 Aggregation is lost when media is replaced with water but is retained when replaced with 1× PBS.
752 Light microscopy (phase contrast) of cells grown overnight in SabDex followed by either
753 replacement of media with ddH_2O, 1× PBS, or ddH_2O followed by 1× PBS. Non-aggregative (Non-
754 Agg) strains were unaffected by the suspension liquid while aggregative (Agg) strains retained
755 aggregation when suspended in 1× PBS, but aggregates were noticeably reduced after washing
756 with ddH_2O. Scale bars represent 50 µm.

757

758

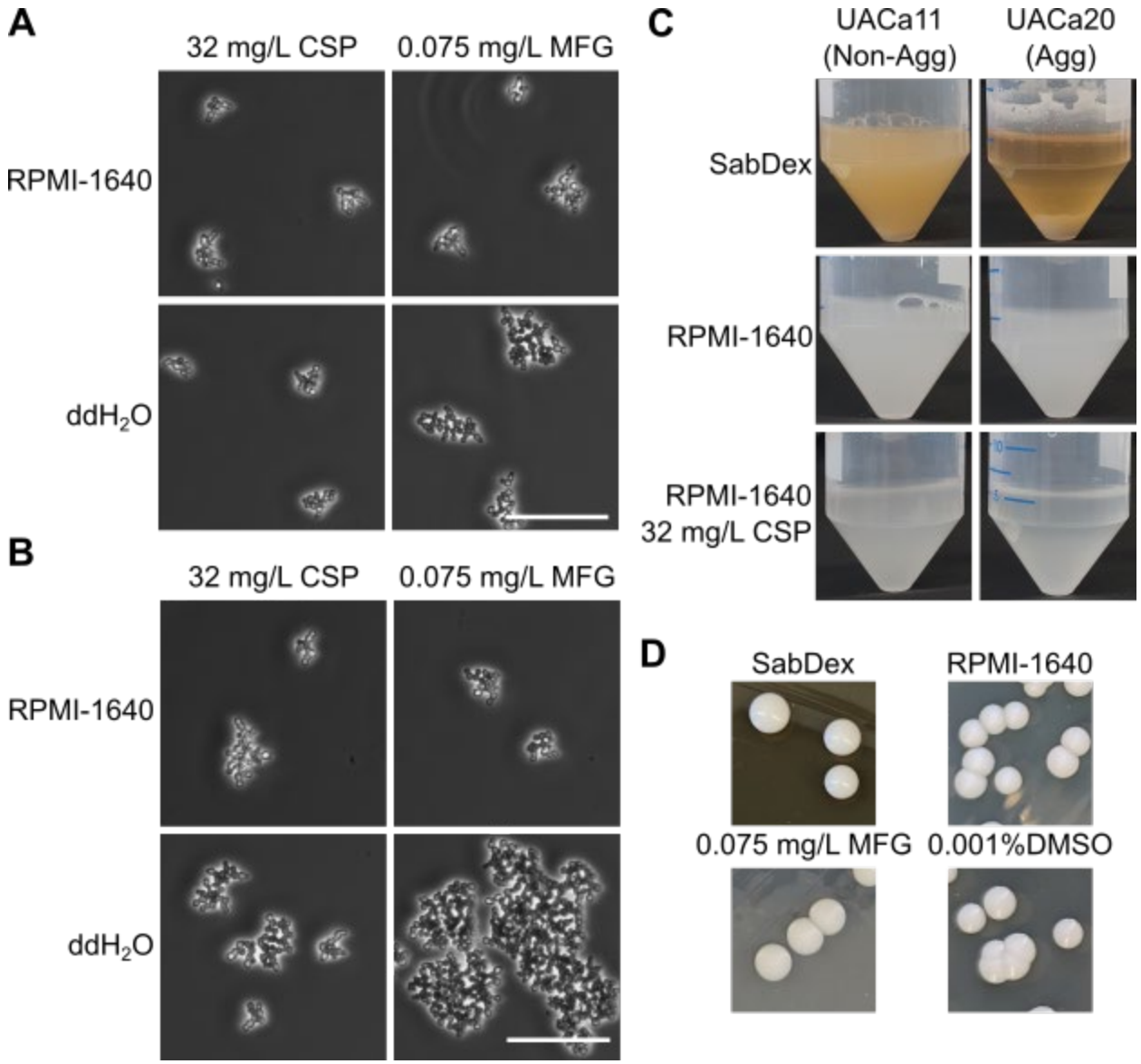

759

760 **Fig 2. Sub-inhibitory concentrations of echinocandins induce a different type of**
761 **aggregation (clustering).** (**A**) UACa20 (clade III) and (**B**) UACa11 (clade I) grown overnight in
762 RPMI-1640 containing either 32 mg/L CSP or 0.075 mg/L MFG, images were taken with a light
763 microscope (phase contrast) of cells in media and when resuspended in ddH_2O, showing drug-
764 induced clusters remain intact after washing with ddH_2O. Scale bars in (A) and (B) represent 50
765 µm. (**C**) Differences in sedimentation were not observed in the RPMI-1640 cultures or the drug-
766 induced clusters, while media-induced aggregates did fall out of suspension. (**D**) Colony
767 morphology was not conspicuously impacted by aggregation.

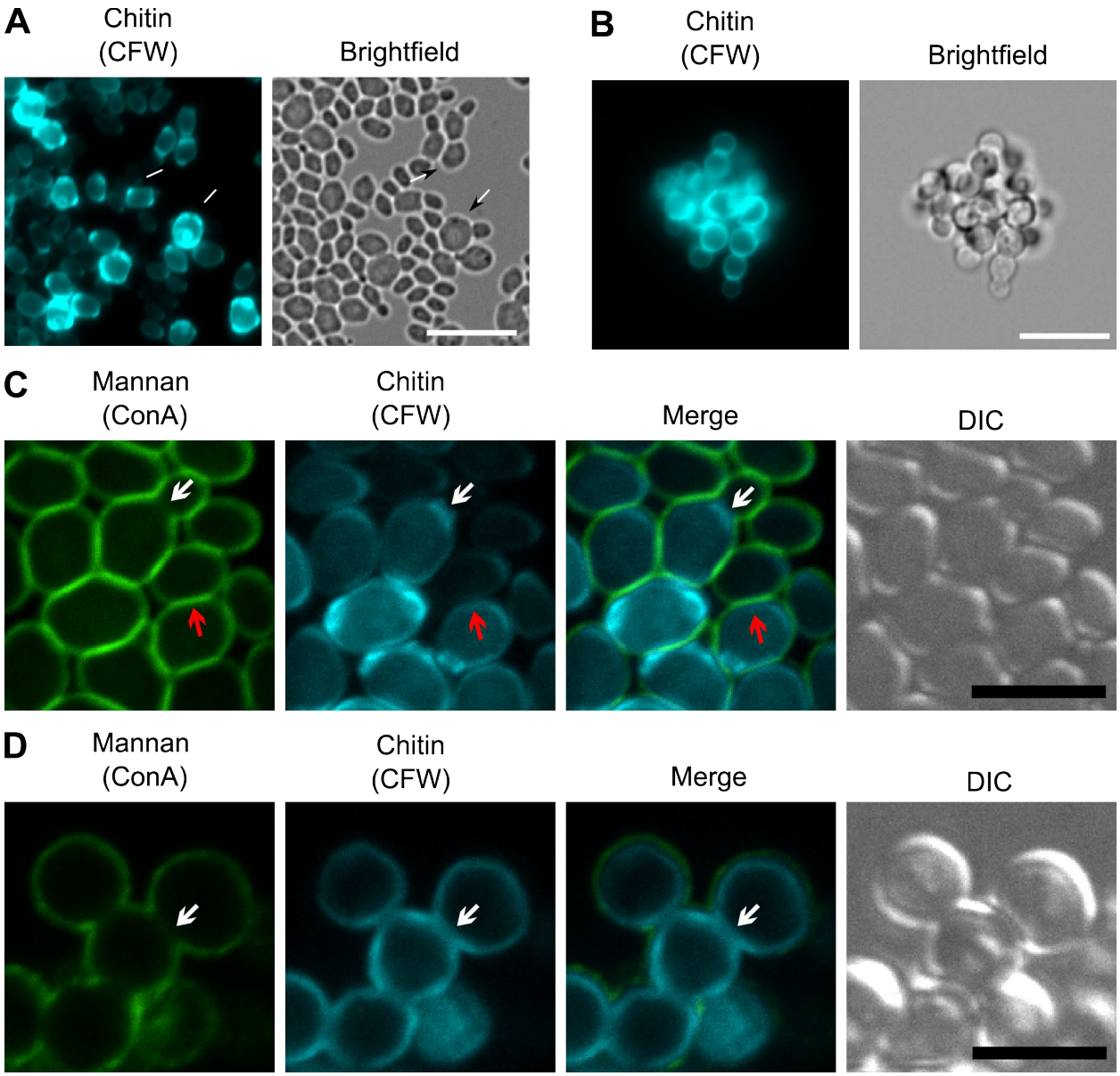

Fig 3. Differences in chitin bud scars and the coverage of outer cell wall mannan indicate differences between aggregation types. (**A, B**) UACa20 (clade III) cells grown overnight in SabDex (A) or RPMI-1640 containing 32 mg/L CSP (B), cell wall chitin is visualized with 10 µg/mL CFW. White arrows point to bud scars without daughter cells grown in SabDex indicating full cell separation after division, this is not seen on antifungal-induced aggregation. Scale bars in (A) and (B) represents 10 µm. (**C, D**) Cell wall mannan and chitin stained with ConA and CFW, respectively, visualized by confocal microscopy to generate image sections of entire aggregates. (**C**) Cells grown in SabDex are completely outlined by mannan and chitin staining (red arrows), even where cells are closely juxtaposed, only actively dividing cells with small daughter buds appear to have a break in the mannan outer cell wall layer (white arrows). (**D**) When grown in RPMI-1640 containing 0.075 mg/L MFG cells are completely bounded by chitin, but display a lack of mannan staining at cell-cell junctions (white arrows) indicating a cell separation defect. In (C) and (D) the scale bars represent 5 µm.

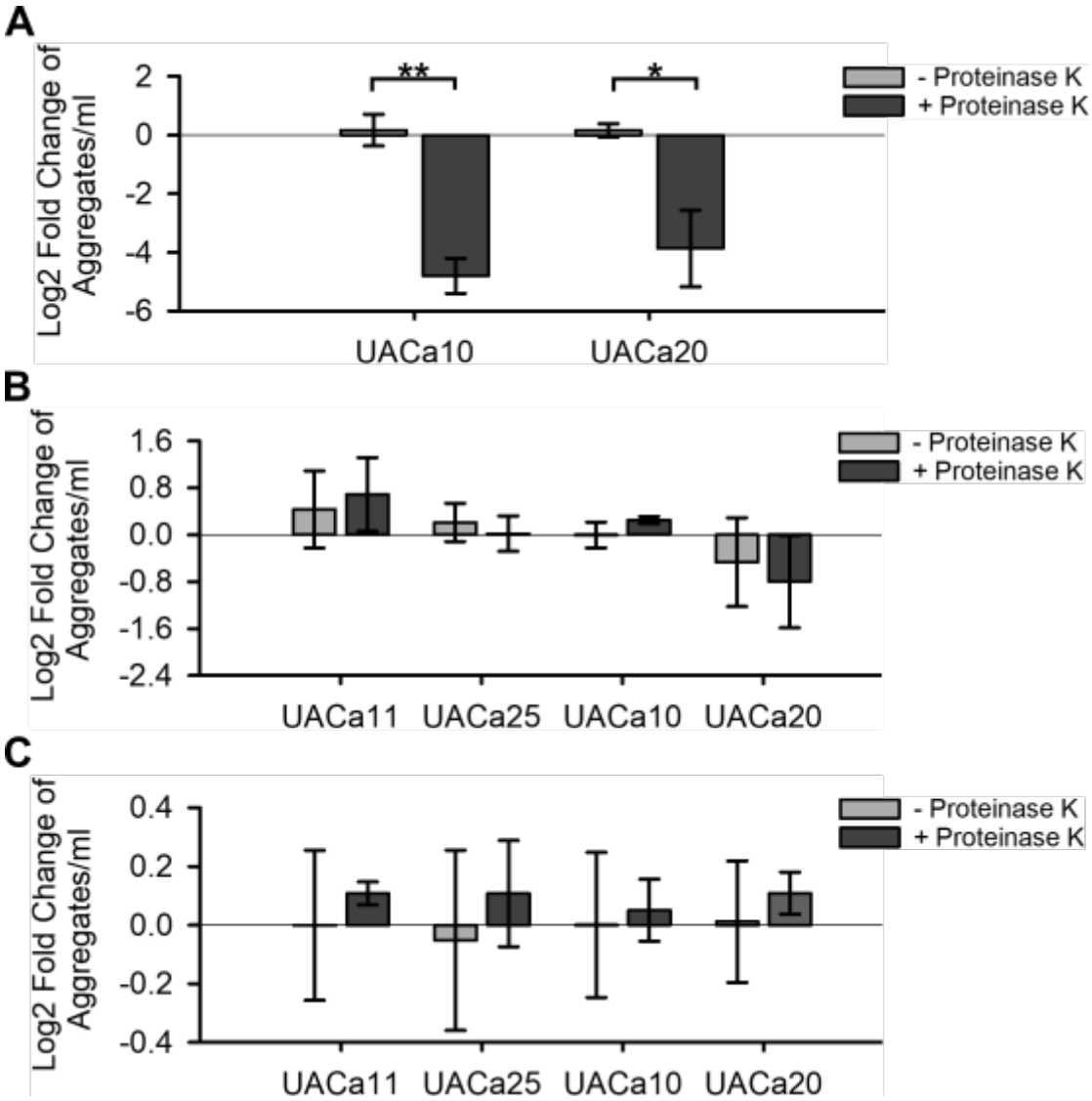

782

783 **Fig 4. Proteinase K treatment significantly reduces media-induced aggregation but not**
784 **antifungal-induced clustering**. Log_2-fold change in aggregate/cluster numbers grown in
785 SabDex (**A**), 32 mg/L CSP (**B**), or 0.075 mg/L MFG (**C**) after incubation at 50 °C for 1 hour with
786 or without 12.5 µg of proteinase K. *$p < 0.05$, **$p < 0.001$, as determined by independent samples
787 t-test.

788

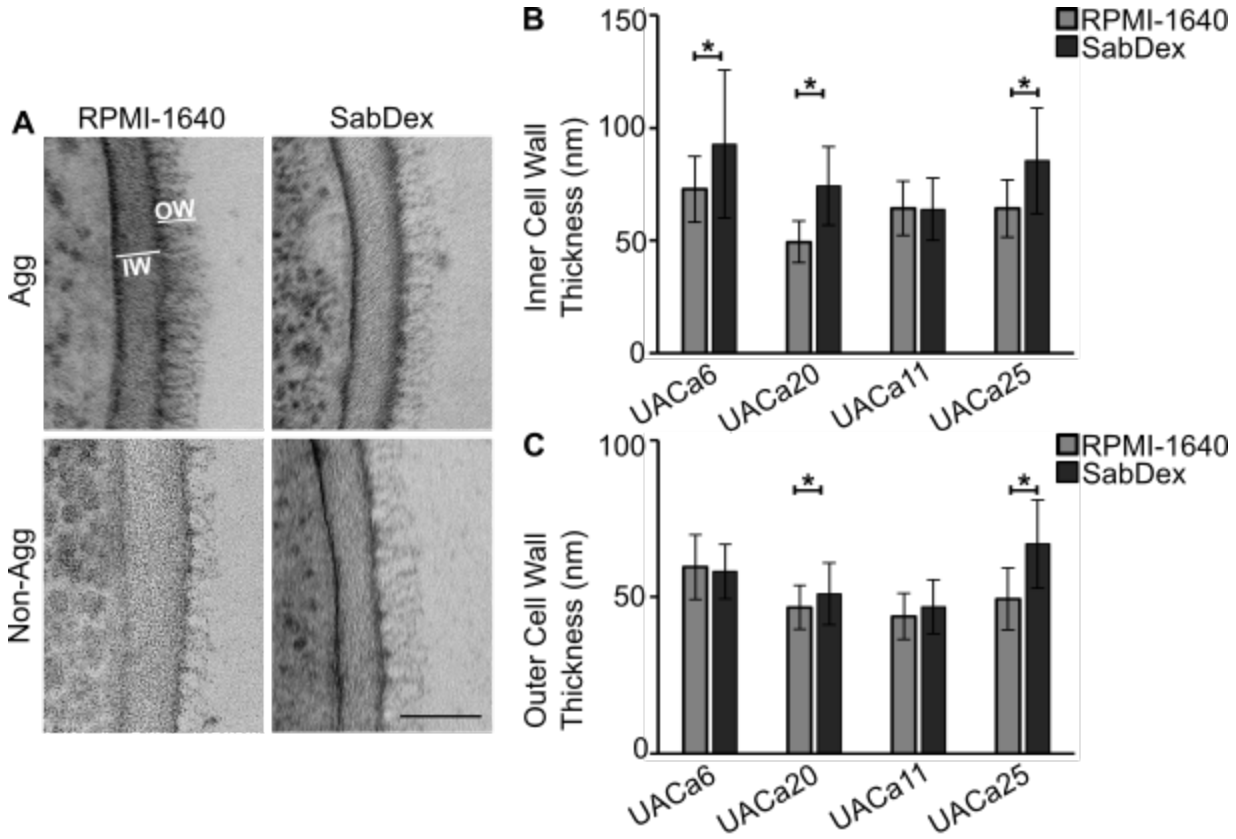

789

790 **Fig 5. Media-induced aggregation does not cause changes to the cell wall ultrastructure.**
791 Cells grown in indicated media were fixed by high pressure freezing for transmission electron
792 microscopy TEM. (**A**) Representative images from TEM of cell wall of an aggregative (Agg) and
793 a non-aggregative (Non-Agg) strain, outer cell wall (OW) and inner cell wall (IW) are indicated.
794 Scale bar represents 50 nm. (**B**) Inner cell wall measurements show strain-specific changes in
795 response to culture conditions. (**C**) Length of mannan fibrils (outer cell wall) shows moderate
796 changes in response to culture conditions in two isolates, UACa20 (clade III) (Agg) and UACa25
797 (clade I) (Non-Agg). *$p < 0.05$ as determined by independent samples t-test.

798

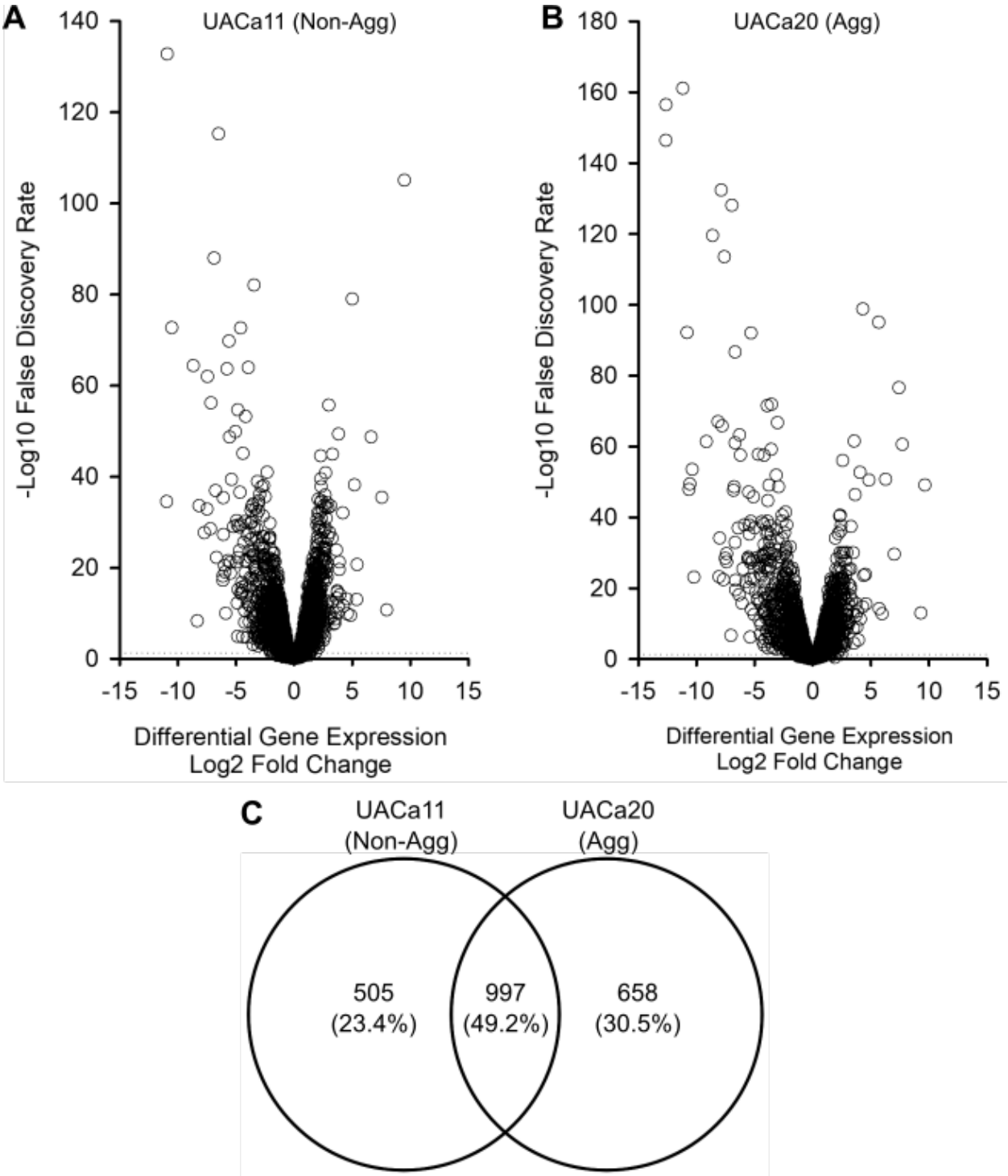

Fig 6. Differential expression of genes (DEGs) in an aggregative and a non-aggregative strain grown in SabDex or RPMI-1640. Aggregative (Agg) clade III strain UACa20 and non-aggregative (Non-Agg) clade I strain UACa11 were grown in the specified media for 16 hours and RNA was extracted for RNA-seq, this was repeated three times on independent colonies at different times. (**A, B**) Volcano plots of the total DEGs for UACa11 (A) and UACa20 (B) are shown with the dotted line indicating an FDR = 0.05. (**C**) Venn diagram of statistically significant (FDR < 0.05) DEGs, numbers indicate how many DEGs are unique to UACa11 and UACa20 and what portion of DEGs are shared between the strains.

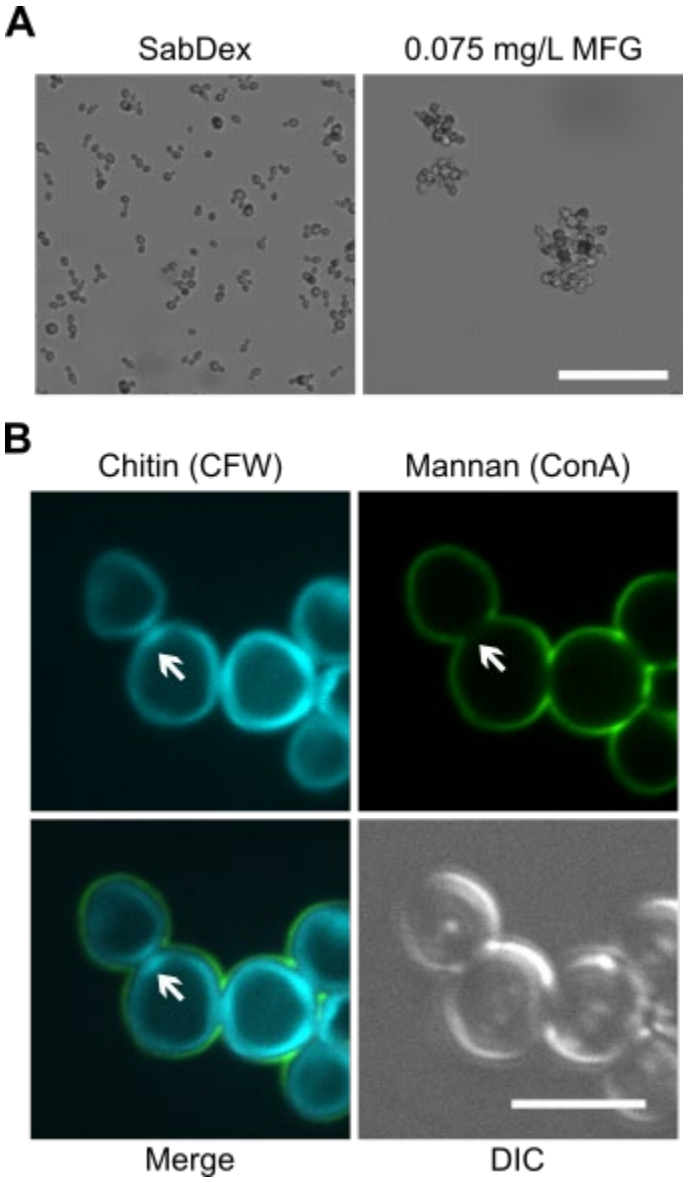

808

809 **Fig 7. *ALS4112* seems to be required for media-induced aggregation, but not for antifungal-**
810 **induced clustering.** (**A**) Light microscopy images (contrast) of the *als4112*Δ mutant grown
811 SabDex or RPMI-1640 containing 0.075 mg/L MFG for 24 hours. Cells grown in SabDex failed to
812 aggregate, whereas cells grown in the presence of MFG did form clusters. Scale bar represent
813 10 µm. (**B**) The *als4112*Δ mutant was grown for 24 hours in RPMI-1640 containing 0.075 mg/L
814 MFG and was imaged by confocal microscopy. Total cell wall chitin was stained with CFW and
815 mannans stained with ConA. White arrows highlight features consistent with antifungal-induced
816 clustering, where cells are completely surrounded by chitin staining, but display a lack of mannan
817 staining at cell-cell junctions. Scale bar represents 5 µm.

818

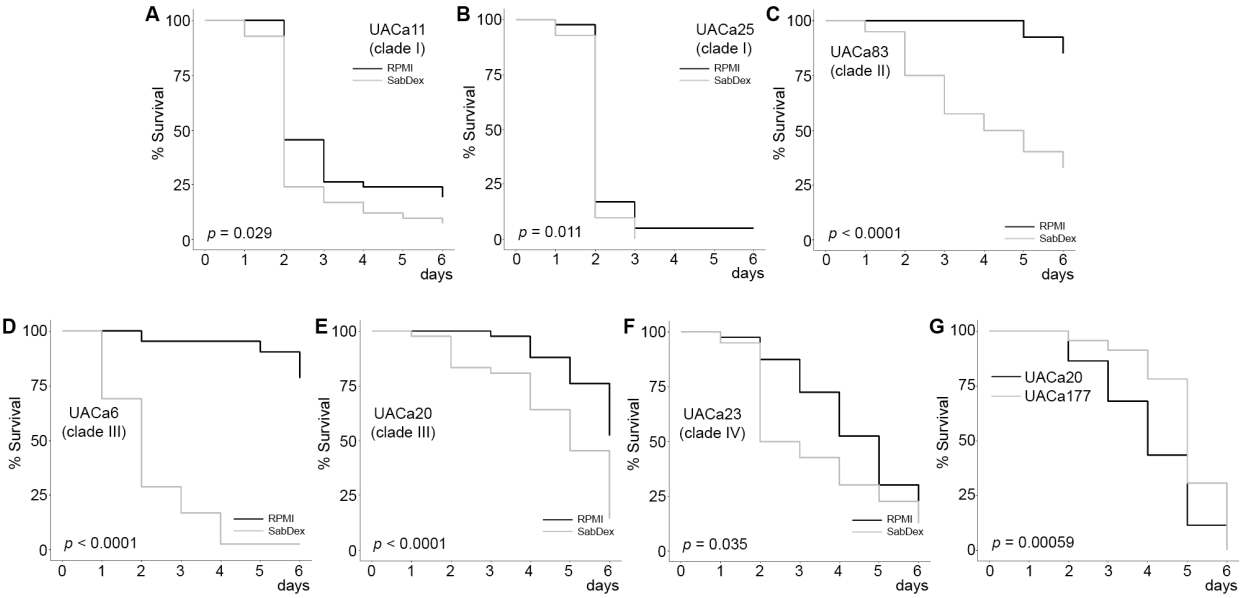

Fig 8. Virulence in the *G. mellonella* infection model is dependent on pre-growth media and Als4112. (**A-C**) Non-aggregative and (**D-F**) aggregative *C. auris* strains were grown in RPMI-1640 or SabDex before inoculation into *G. mellonella* larvae. All strains except UACa25 (clade I) in (B) showed significant differences in virulence dependent on the media used to grow the fungal cells before inoculation. (**G**) Wild-type (UACa20) and *als4112*Δ (UACa177) *C. auris* cells were grown in SabDex before inoculation into *G. mellonella* larvae (A log-rank test was used to calculate *p*-values . 30 larvae in 3 independent experiments were used to assess virulence.

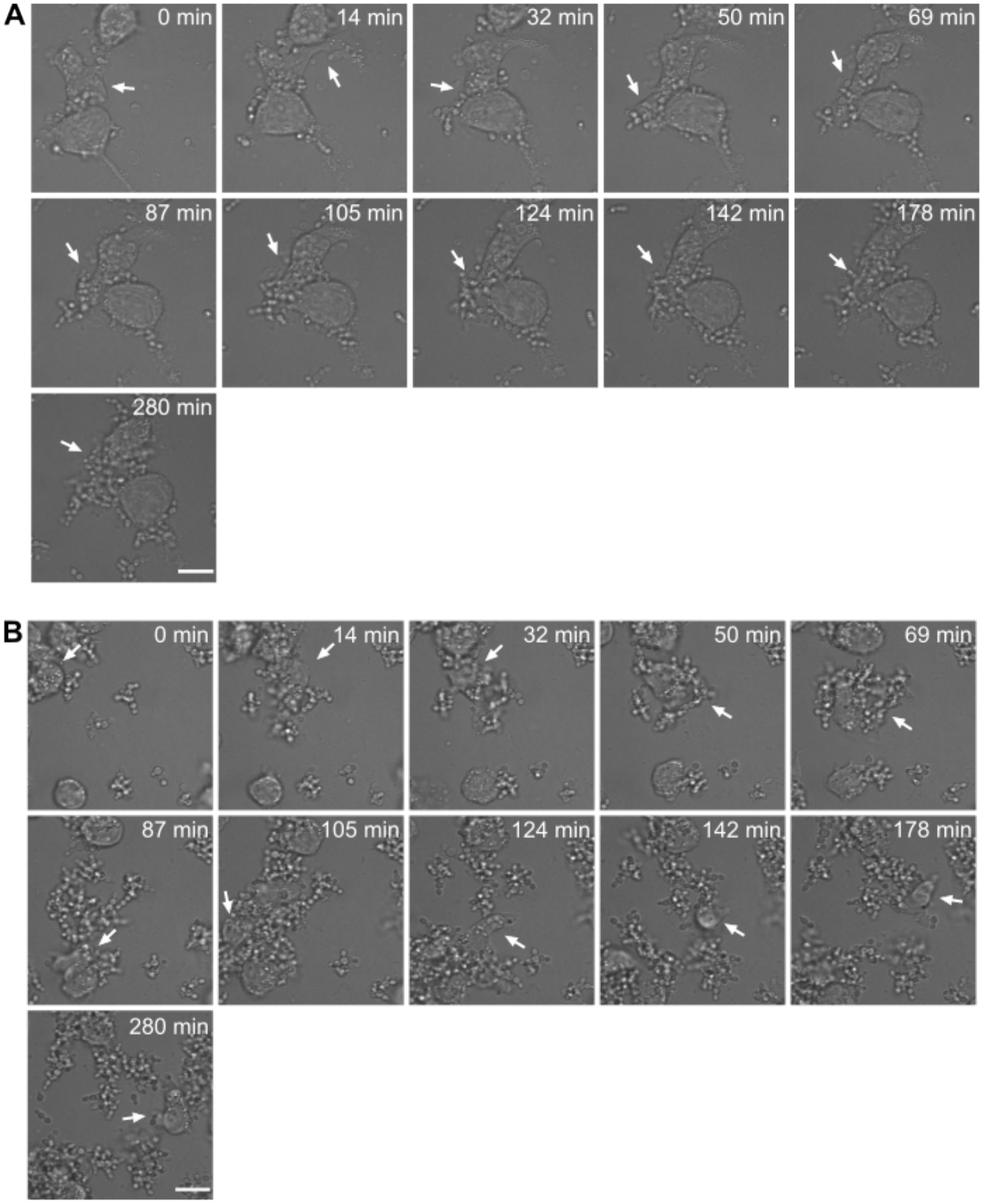

828

829 **Fig 9. Macrophages have difficulty in clearing large aggregates and clusters.** (**A**)
830 Aggregates of strain UACa20 (clade III) grown in SabDex were co-incubated with THP-1 derived
831 macrophages, and one macrophage was followed for the duration of the experiment (white arrow),
832 taken from Video V3. (**B**) Clusters of strain UACa20 grown in RPMI-1640 containing 0.075 mg/L

833 MFG, one macrophage was followed for the duration of the experiment (white arrow), taken from
834 Video V4. Scale bars represent 15 µm.

835

836 **References**

837 1. Satoh K, Makimura K, Hasumi Y, Nishiyama Y, Uchida K, Yamaguchi H.
838 *Candida auris* sp. nov., a novel ascomycetous yeast isolated from the
839 external ear canal of an inpatient in a Japanese hospital. Microbiol
840 Immunol. 2009;53: 41–44. doi:10.1111/j.1348-0421.2008.00083.x

841 2. Rhodes J, Fisher MC. Global epidemiology of emerging *Candida auris*. Curr
842 Opin Microbiol. 2019;52: 84–89. doi:10.1016/j.mib.2019.05.008

843 3. Forsberg K, Woodworth K, Walters M, Berkow EL, Jackson B, Chiller T, et
844 al. *Candida auris*: The recent emergence of a multidrug-resistant fungal
845 pathogen. Med Mycol. 2019;57: 1–12. doi:10.1093/mmy/myy054

846 4. Stephenson JC, Garza DR, Bouklas T. A fungus for our time: *Candida auris*
847 emerges into the anthropocene. Curr Trop Med Rep. 2023.
848 doi:10.1007/s40475-023-00293-w

849 5. Lockhart SR, Etienne KA, Vallabhaneni S, Farooqi J, Chowdhary A,
850 Govender NP, et al. Simultaneous emergence of multidrug-resistant
851 *Candida auris* on 3 continents confirmed by whole-genome sequencing and
852 epidemiological analyses. Clinical Infectious Diseases. 2017;64: 134–140.
853 doi:10.1093/cid/ciw691

854 6. Chow NA, de Groot T, Badali H, Abastabar M, Chiller TM, Meis JF.
855 Potential fifth clade of *Candida auris*, Iran, 2018. Emerg Infect Dis. 2019;25:
856 1780–1781. doi:10.3201/eid2509.190686

857 7. Arastehfar A, Shaban T, Zarrinfar H, Roudbary M, Ghazanfari M, Hedayati
858 M-T, et al. Candidemia among Iranian patients with severe COVID-19
859 admitted to ICUs. Journal of Fungi. 2021;7: 280. doi:10.3390/jof7040280

860 8. Noble SM, Gianetti BA, Witchley JN. *Candida albicans* cell-type switching
861 and functional plasticity in the mammalian host. Nat Rev Microbiol. 2017;15:
862 96–108. doi:10.1038/nrmicro.2016.157

863 9. Iracane E, Vega-Estévez S, Buscaino A. On and Off: epigenetic regulation
864 of *C. albicans* morphological switches. Pathogens. 2021;10: 1463.
865 doi:10.3390/pathogens10111463

866 10. Kumamoto CA, Vinces MD. Contributions of hyphae and hypha-co-
867 regulated genes to *Candida albicans* virulence. Cell Microbiol. 2005;7:
868 1546–1554. doi:10.1111/j.1462-5822.2005.00616.x

869 11. Yue H, Bing J, Zheng Q, Zhang Y, Hu T, Du H, et al. Filamentation in
870 *Candida auris*, an emerging fungal pathogen of humans: passage through
871 the mammalian body induces a heritable phenotypic switch. Emerg
872 Microbes Infect. 2018;7: 188. doi:10.1038/s41426-018-0187-x

873 12. Bravo Ruiz G, Ross ZK, Gow NAR, Lorenz A. Pseudohyphal growth of the
874 emerging pathogen *Candida auris* is triggered by genotoxic stress through

875 the S phase checkpoint. mSphere. 2020;5: e00151-20.
876 doi:10.1128/msphere.00151-20

877 13. Borman AM, Szekely A, Johnson EM. Comparative pathogenicity of United
878 Kingdom isolates of the emerging pathogen *Candida auris* and other key
879 pathogenic *Candida* species. mSphere. 2016;1: e00189-16.
880 doi:10.1128/mSphere.00189-16

881 14. Santana DJ, O'Meara TR. Forward and reverse genetic dissection of
882 morphogenesis identifies filament-competent *Candida auris* strains. Nat
883 Commun. 2021;12: 7197. doi:10.1038/s41467-021-27545-5

884 15. Zamith-Miranda D, Amatuzzi RF, Munhoz da Rocha IF, Martins ST, Lucena
885 ACR, Vieira AZ, et al. Transcriptional and translational landscape of
886 *Candida auris* in response to caspofungin. Comput Struct Biotechnol J.
887 2021;19: 5264–5277. doi:10.1016/j.csbj.2021.09.007

888 16. Szekely A, Borman AM, Johnson EM. *Candida auris* isolates of the
889 Southern Asian and South African lineages exhibit different phenotypic and
890 antifungal susceptibility profiles *in vitro*. J Clin Microbiol. 2019;57: e02055-
891 18. doi:10.1128/jcm.02055-18

892 17. Bing J, Guan Z, Zheng T, Zhang Z, Fan S, Ennis CL, et al. Clinical isolates
893 of *Candida auris* with enhanced adherence and biofilm formation due to
894 genomic amplification of *ALS4*. Cramer RA, editor. PLoS Pathog. 2023;19:
895 e1011239. doi:10.1371/journal.ppat.1011239

896 18. Forgács L, Borman AM, Prépost E, Tóth Z, Kovács R, Szekely A, et al.
897 Comparison of *in vivo* pathogenicity of four *Candida auris* clades in a
898 neutropenic bloodstream infection murine model. Emerg Infect Dis. 2020;9:
899 1160–1169. doi:10.1080/22221751.2020.1771218

900 19. Bravo Ruiz G, Lorenz A. What do we know about the biology of the
901 emerging fungal pathogen of humans *Candida auris*? Microbiol Res.
902 2021;242: 126621. doi:10.1016/j.micres.2020.126621

903 20. Malavia-Jones D, Farrer RA, Stappers MHT, Edmondson MB, Borman AM,
904 Johnson EM, et al. Strain and temperature dependent aggregation of
905 *Candida auris* is attenuated by inhibition of surface amyloid proteins. The
906 Cell Surface. 2023; DOI: 10.1016/j.tcsw.2023.100110.
907 doi:10.1016/j.tcsw.2023.100110

908 21. Ramos LS, Parra-Giraldo CM, Branquinha MH, Santos ALS. Cell
909 aggregation capability of clinical isolates from *Candida auris* and *Candida*
910 *haemulonii* species complex. Trop Med Infect Dis. 2023;8: 382.
911 doi:10.3390/tropicalmed8080382

912 22. Short B, Brown J, Delaney C, Sherry L, Williams C, Ramage G, et al.
913 *Candida auris* exhibits resilient biofilm characteristics *in vitro*: implications
914 for environmental persistence. Journal of Hospital Infection. 2019;103: 92–
915 96. doi:10.1016/j.jhin.2019.06.006

916 23. Singh R, Kaur M, Chakrabarti A, Shankarnarayan SA, Rudramurthy SM.
917 Biofilm formation by *Candida auris* isolated from colonising sites and
918 candidemia cases. Mycoses. 2019;62: 706–709. doi:10.1111/myc.12947

919 24. Romera D, Aguilera-Correa J-J, García-Coca M, Mahillo-Fernández I,
920 Viñuela-Sandoval L, García-Rodríguez J, et al. The *Galleria mellonella*
921 infection model as a system to investigate the virulence of *Candida auris*
922 strains. Pathog Dis. 2020;78: ftaa067. doi:10.1093/femspd/ftaa067

923 25. Biswas B, Gangwar G, Nain V, Gupta I, Thakur A, Puria R. Rapamycin and
924 Torin2 inhibit *Candida auris* TOR: Insights through growth profiling, docking,
925 and MD simulations. J Biomol Struct Dyn. 2022.
926 doi:10.1080/07391102.2022.2134927

927 26. Hoyer LL, Cota E. *Candida albicans* Agglutinin-like sequence (Als) family
928 vignettes: a review of Als protein structure and function. Front Microbiol.
929 2016;7: 280. doi:10.3389/fmicb.2016.00280

930 27. Muñoz JF, Gade L, Chow NA, Loparev VN, Juieng P, Berkow EL, et al.
931 Genomic insights into multidrug-resistance, mating and virulence in
932 *Candida auris* and related emerging species. Nat Commun. 2018;9: 5346.
933 doi:10.1038/s41467-018-07779-6

934 28. Muñoz JF, Welsh RM, Shea T, Batra D, Gade L, Howard D, et al. Clade-
935 specific chromosomal rearrangements and loss of subtelomeric adhesins in
936 *Candida auris*. Mitchell A, editor. Genetics. 2021;218: iyab029.
937 doi:10.1093/genetics/iyab029

938 29. Singh S, Uppuluri P, Mamouei Z, Alqarihi A, Elhassan H, French S, et al.
939 The NDV-3A vaccine protects mice from multidrug resistant *Candida auris*
940 infection. PLoS Pathog. 2019;15: e1007460.
941 doi:10.1371/journal.ppat.1007460

942 30. Smoak RA, Snyder LF, Fassler JS, He BZ. Parallel expansion and
943 divergence of an adhesin family in pathogenic yeasts. Genetics. 2023;223:
944 iyad024. doi:10.1093/genetics/iyad024

945 31. Santana DJ, Anku JAE, Zhao G, Zarnowski R, Johnson CJ, Hautau H, et al.
946 A *Candida auris* –specific adhesin, Scf1, governs surface association,
947 colonization, and virulence. Science (1979). 2023;381: 1461–1467.
948 doi:10.1126/science.adf8972

949 32. Liu Y, Filler SG. *Candida albicans* Als3, a multifunctional adhesin and
950 invasin. Eukaryot Cell. 2011;10: 168–173. doi:10.1128/EC.00279-10

951 33. Willaert R. Adhesins of yeasts: protein structure and interactions. Journal of
952 Fungi. 2018;4: 119. doi:10.3390/jof4040119

953 34. Mayr E-M, Ramírez-Zavala B, Krüger I, Morschhäuser J. A Zinc Cluster
954 transcription factor contributes to the intrinsic fluconazole resistance of
955 *Candida auris*. Mitchell AP, editor. mSphere. 2020;5: e00279-20.
956 doi:10.1128/mSphere.00279-20

957 35. Garcia-Bustos V, Ruiz-Saurí A, Ruiz-Gaitán A, Sigona-Giangreco IA,
958 Cabañero-Navalon MD, Sabalza-Baztán O, et al. Characterization of the
959 differential pathogenicity of *Candida auris* in a *Galleria mellonella* infection

960 model. Microbiol Spectr. 2021;9: e00013-21. doi:10.1128/Spectrum.00013-
961 21

962 36. Ene I V., Adya AK, Wehmeier S, Brand AC, MacCallum DM, Gow NAR, et
963 al. Host carbon sources modulate cell wall architecture, drug resistance and
964 virulence in a fungal pathogen. Cell Microbiol. 2012;14: 1319–1335.
965 doi:10.1111/j.1462-5822.2012.01813.x

966 37. Leach MD, Farrer RA, Tan K, Miao Z, Walker LA, Cuomo CA, et al. Hsf1
967 and Hsp90 orchestrate temperature-dependent global transcriptional
968 remodelling and chromatin architecture in Candida albicans. Nat Commun.
969 2016;7: 11704. doi:10.1038/ncomms11704

970 38. Thompson DS, Carlisle PL, Kadosh D. Coevolution of morphology and
971 virulence in *Candida* species. Eukaryot Cell. 2011;10: 1173–1182.
972 doi:10.1128/EC.05085-11

973 39. Brown AJP, Brown GD, Netea MG, Gow NAR. Metabolism impacts upon
974 *Candida* immunogenicity and pathogenicity at multiple levels. Trends
975 Microbiol. 2014;22: 614–622. doi:10.1016/j.tim.2014.07.001

976 40. Lorenz A, Papon N. New tools for the new bug *Candida auris*. Trends
977 Microbiol. 2022;30: 203–205. doi:10.1016/j.tim.2022.01.010

978 41. Wang Y, Zou Y, Chen X, Li H, Yin Z, Zhang B, et al. Innate immune
979 responses against the fungal pathogen *Candida auris*. Nat Commun.
980 2022;13: 3553. doi:10.1038/s41467-022-31201-x

981 42. Milne G, Walker LA. High-pressure freezing and transmission electron
982 microscopy to visualize the ultrastructure of the *C. auris* cell wall. Methods
983 in Molecular Biology. 2022;2517: 189–201. doi:10.1007/978-1-0716-2417-
984 3_15

985 43. Schindelin J, Arganda-Carreras I, Frise E, Kaynig V, Longair M, Pietzsch T,
986 et al. Fiji: an open-source platform for biological-image analysis. Nat
987 Methods. 2012;9: 676–682. doi:10.1038/nmeth.2019

988 44. The External RNA Controls Consortium. The External RNA Controls
989 Consortium: a progress report. Nat Methods. 2005;2: 731–734.
990 doi:10.1038/nmeth1005-731

991 45. Kim D, Langmead B, Salzberg SL. HISAT: a fast spliced aligner with low
992 memory requirements. Nat Methods. 2015;12: 357–360.
993 doi:10.1038/nmeth.3317

994 46. Chatterjee S, Alampalli SV, Nageshan RK, Chettiar ST, Joshi S, Tatu US.
995 Draft genome of a commonly misdiagnosed multidrug resistant pathogen
996 *Candida auris*. BMC Genomics. 2015;16: 686. doi:10.1186/s12864-015-
997 1863-z

998 47. Li H, Handsaker B, Wysoker A, Fennell T, Ruan J, Homer N, et al. The
999 Sequence Alignment/Map format and SAMtools. Bioinformatics. 2009;25:
1000 2078–2079. doi:10.1093/bioinformatics/btp352

1001 48. Liao Y, Smyth GK, Shi W. featureCounts: an efficient general purpose
1002 program for assigning sequence reads to genomic features. Bioinformatics.
1003 2014;30: 923–930. doi:10.1093/bioinformatics/btt656

1004 49. Robinson MD, McCarthy DJ, Smyth GK. <tt>edgeR</tt> : a Bioconductor
1005 package for differential expression analysis of digital gene expression data.
1006 Bioinformatics. 2010;26: 139–140. doi:10.1093/bioinformatics/btp616

1007 50. Camacho C, Coulouris G, Avagyan V, Ma N, Papadopoulos J, Bealer K, et
1008 al. BLAST+: architecture and applications. BMC Bioinformatics. 2009;10:
1009 421. doi:10.1186/1471-2105-10-421

1010 51. Bravo Ruiz G, Lorenz A. Genetic transformation of *Candida auris* via
1011 homology-directed repair using a standard lithium acetate protocol.
1012 Methods in Molecular Biology. 2022;2517: 95–110. doi:10.1007/978-1-
1013 0716-2417-3_8

1014 52. Daigneault M, Preston JA, Marriott HM, Whyte MKB, Dockrell DH. The
1015 identification of markers of macrophage differentiation in PMA-stimulated
1016 THP-1 cells and monocyte-derived macrophages. PLoS One. 2010;5:
1017 e8668. doi:10.1371/journal.pone.0008668

1018